

# AN ALGEBRAIC SPARSIFIED NESTED DISSECTION ALGORITHM USING LOW-RANK APPROXIMATIONS

LÉOPOLD CAMBIER\*, CHAO CHEN†, ERIK G. BOMAN ‡, SIVASANKARAN  
RAJAMANICKAM§, RAYMOND S. TUMINARO¶, AND ERIC DARVE||

**Abstract.** We propose a new algorithm for the fast solution of large, sparse, symmetric positive-definite linear systems, spaND — sparsified Nested Dissection. It is based on nested dissection, sparsification and low-rank compression. After eliminating all interiors at a given level of the elimination tree, the algorithm sparsifies all separators corresponding to the interiors. This operation reduces the size of the separators by eliminating some degrees of freedom but without introducing any fill-in. This is done at the expense of a small and controllable approximation error. The result is an approximate factorization that can be used as an efficient preconditioner. We then perform several numerical experiments to evaluate this algorithm. We demonstrate that a version using orthogonal factorization and block-diagonal scaling takes less CG iterations to converge than previous similar algorithms on various kinds of problems. Furthermore, this algorithm is provably guaranteed to never break down and the matrix stays symmetric positive-definite throughout the process. We evaluate the algorithm on some large problems show it exhibits near-linear scaling. The factorization time is roughly  $\mathcal{O}(N)$  and the number of iterations grows slowly with  $N$ .

**Key words.** sparse linear solver, hierarchical matrix, nested dissection, preconditioner, low-rank

**AMS subject classifications.** 65F05, 65F08, 65Y20

**1. Introduction.** We are interested in solving large symmetric, positive-definite (SPD) sparse linear systems

$$(1.1) \quad Ax = b, \quad A \in \mathbb{R}^{N \times N}.$$

In particular, we focus on linear systems with similar properties as those arising from the discretization of elliptic partial differential equations, using finite difference or finite elements for instance. Solving such systems is a crucial part of many scientific simulations.

Algorithms for solving Eq. 1.1 are traditionally divided into three categories. On one hand are direct methods. The naive Cholesky ( $A = LL^T$ ) factorization can lead to a factorization cost of  $\mathcal{O}(N^3)$  due to fill-in in the factor  $L$ . When the matrix  $A$  comes from the discretization of PDE's in 2D or 3D space, one usually uses the Nested Dissection [39] ordering to reduce fill-in. By doing so, the complexity is typically reduced to  $\mathcal{O}(N^{3/2})$  (in 2D) and  $\mathcal{O}(N^2)$  (in 3D) [24, 39]. This is what most state-of-the-art direct solvers are built upon [16, 3, 34]. Those algorithm work very well for most moderate-size problems. However, the  $\mathcal{O}(N^2)$  complexity in 3D makes them intractable on large scale problems.

An alternative is to use iterative algorithms like Krylov methods or multigrid. Multigrid [22, 9, 31] (and its algebraic version, [10, 49]) works very well on fairly regular elliptic PDE's, usually with a near-constant iteration count regardless of the problem size. However, it can solve only a fairly limited range of problems and its

\*Institute for Computational & Mathematical Engineering, Stanford University, [lcambier@stanford.edu](mailto:lcambier@stanford.edu), <https://people.stanford.edu/lcambier>

†Institute for Computational Engineering and Sciences, The University of Texas at Austin, [chen-chao.nk@gmail.com](mailto:chen-chao.nk@gmail.com)

‡Center for Computing Research, Sandia National Laboratories, [egboman@sandia.gov](mailto:egboman@sandia.gov)

§Center for Computing Research, Sandia National Laboratories, [srajama@sandia.gov](mailto:srajama@sandia.gov)

¶Center for Computing Research, Sandia National Laboratories, [rstumin@sandia.gov](mailto:rstumin@sandia.gov)

||Department of Mechanical Engineering, Stanford University, [darve@stanford.edu](mailto:darve@stanford.edu)

iteration count can start growing when the problem becomes ill-conditioned. Krylov methods, such as CG [35, 51], MINRES [41] or GMRES [46] can be applied to a very wide range of problems, necessitating only sparse matrix-vector products. However, to converge at all, one needs to always couple them with an efficient preconditioner. This is typically a very problem dependent task.

One way, however, to build preconditioners is using incomplete factorizations and low-rank approximations. Incomplete factorization algorithms are built on top of a classical matrix factorization algorithm. Incomplete LU (ILU) for instance starts with a classical LU algorithm and ignores some of the fill-in based on thresholding and on an artificially prescribed maximum number of non-zeroes in every row & column [44]. Block versions [47] are sometimes used because of better robustness (with possible pivoting) and practical properties (cache-friendly algorithm, use of BLAS, etc.). Once an incomplete LU factorization has been computed, it can be used as a preconditioner for a CG or GMRES algorithm for instance.

Matrices arising from PDE discretization also typically have low-rank off-diagonal blocks [7, 6, 13]. More precisely, the fill-in arising when factoring the matrix typically has small numerical rank, with weak dependence on  $N$ . This is closely related to the existence of a smooth Green's function for the underlying PDE and to the Fast Multipole Method [5, 28, 23]. Matrices built using this property are broadly called Hierarchical ( $\mathcal{H}$ ) matrices [30]. Many formats exist, depending on when and how off-diagonal blocks are compressed into low-rank format. The Hierarchical Off-Diagonal Low Rank (HODLR) [1] format compresses all off-diagonal blocks. If the off-diagonal are compressed using a nested basis, we obtain Hierarchically Semi-Separable (HSS) matrices [14, 12, 15, 55]. Finally, the broader category of  $\mathcal{H}^2$  matrices also uses nested basis but only compresses well-separated (i.e., far-field) interactions [32, 33, 42, 58]. All of those representations lead to a data-sparse representation of the matrix with tunable accuracy (by making the low-rank approximations more or less accurate) and fast inverse computations. This can then be used to construct preconditioners. These constructions, while asymptotically efficient, sometimes have fairly large constants.

Attempts to improve the practical performance rely on exploiting sparsity as well as the low rank structure. Most approaches up-to-date have focused on incorporating fast (i.e.,  $\mathcal{H}$ -) algebra into the classical Nested Dissection algorithm [27] in order to decrease the cost of working with large fronts. Other work have taken the similar approach of incorporating rank structured matrices into a multifrontal factorization in order to compress the large dense frontal matrices. [54, 48, 52, 53, 25] all use HSS to compress the large frontal matrices. The last one was incorporated into the Strumpack package. [2] uses Block Low-Rank approximation to compress the frontal matrices in the MUMPS solver [3]. Finally, [21] studies the use of  $\mathcal{H}$ -matrices using HODLR in the PaStiX solver [34].

The Hierarchical Interpolative Factorization (HIF) [36] proposes a different approach. Instead of storing the full dense fronts in some low-rank format, it uses low-rank approximation to directly sparsify (i.e., eliminate part of) the Nested Dissection separators without introducing any fill-in. As a result, the algorithm never deals with large edges (in low-rank format or not) but instead constantly reduces the size of all edges and separators. This is the approach we take.

We finally mention some recent work by J. Xia & Z. Xin [57], in which a scale-and-compress approach is taken. Our algorithm share some similarities with this, as we also scale the matrix block using the Cholesky factorization of the pivot. As we will see, this significantly improves the preconditioner's accuracy.

**1.1. Contribution.** Our approach is based on the idea of HIF described in [36]. However, there are several differences, improvements and novel capabilities:

- Our algorithm is completely general, and can be applied to any (SPD) matrix. The only required input is the sparse matrix itself. If geometry information is available, it can be used to improved the quality of the ordering & clustering.
- We incorporate an additional diagonal block scaling step in the algorithm, greatly improving the accuracy of the preconditioner for only a small additional cost;
- We use an orthogonal (instead of interpolative) transformation, improving stability and guaranteeing that the preconditioner stays SPD when A is SPD;
- We test the algorithm on more and larger test problems.

In a nutshell, our algorithm is based on a couple of key ideas. First, we start with a nested dissection (ND) ordering. Then following the idea introduced in [36], after each elimination step, we sparsify the interfaces between just-eliminated interiors, effectively reducing the size of *all* ND separators. This is done using low-rank approximation, allowing to sparsify the separators without introducing any fill-in. We then merge clusters and proceed to the next level.

A natural consequence of the above algorithm is that, if the compression fails to reduce the size of the separators, the algorithm reverts to a (slower, but still relatively efficient) Nested Dissection algorithm.

**1.2. Contrast with fast-algebra based algorithms.** We emphasize that the HIF approach [36] is different from the classical way of accelerating sparse direct solvers. Consider for instance the top-separator of a Nested Dissection elimination. At the end of the elimination, the corresponding (very large) block in the matrix is typically dense. MUMPS [2] and PaStiX [21] for instance use fast  $\mathcal{H}$ -algebra to compress this block. This allows for fast factorization, inversion, etc.

As indicated above, we take a different approach. Instead of storing large blocks (corresponding to large separators) in low-rank format, we eliminate part of the separators right from the beginning, effectively reducing their size. We do so without introducing any fill-in, but at the expense of an approximate factorization. As a result, the top-separator stays dense but is much smaller than at the beginning.

**1.3. Organization of the paper.** This paper is organized in three sections. First, [section 2](#) introduces and motivates the algorithm, starting at a high level and later introducing the details. Then, [section 3](#) proves the stability of the scheme and discusses the choice of the low-rank approximation. Finally, [section 4](#) shows numerical experiments on medium and large scale matrices.

**2. Sparsified Nested Dissection.** This section describes the algorithm in detail. We start by discussing Nested Dissection and some of its characteristics. Then, building upon it, we introduce our algorithm, and then detail all the various parts.

**2.1. Classical Nested Dissection Ordering.** Nested Dissection (ND) [24] is an ordering strategy to factor sparse matrices. Consider a sparse symmetric matrix  $A \in \mathbb{R}^{N \times N}$  and its graph  $G_A = (V, E)$  defined as  $V = \{1, \dots, N\}$  and  $E = \{(i, j) : A_{ij} \neq 0\}$ . Notice that since  $A$  is symmetric, the graph is undirected. The basic building block of ND is the computation of *vertex-separators*. Starting with the full graph, one finds a cluster of vertices, a vertex-separator, separating the graph into two disconnected clusters (a cluster is a subset of  $V$ ).

[Fig. 2.1b](#) gives an example of such a separator. The idea is then applied recursively as indicated in [Fig. 2.1c](#) and [Fig. 2.1d](#). That is, disconnected clusters are further

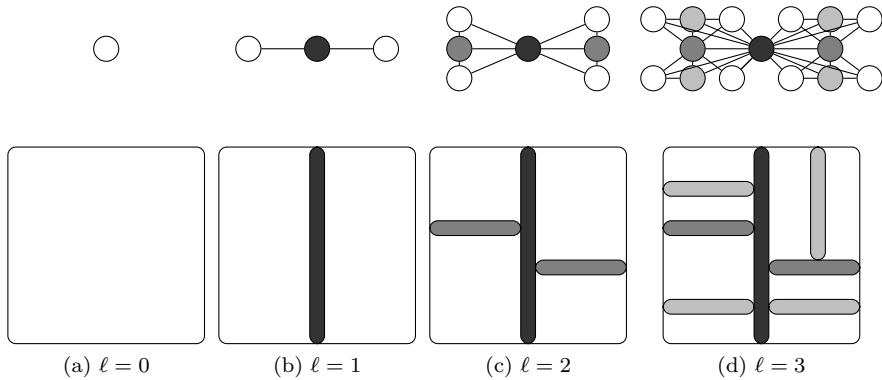


Fig. 2.1: Classical Nested Dissection ordering.

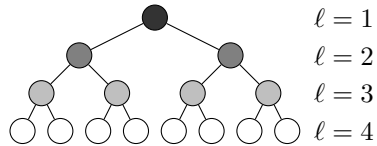


Fig. 2.2: The elimination tree associated to the ND ordering on Fig. 2.1

sub-divided using separators. This recursive process is repeated until cluster sizes are small enough to be factored using some direct dense method. A matrix factorization can begin by eliminating unknowns in all disconnected clusters defined by the last recursive level of the nested dissection process. Thus, the only non-eliminated unknowns correspond to degrees-of-freedom (dofs) associated with all of the separators. We then proceed to eliminate all dofs associated with the last set of separators (e.g., those defined in the  $\ell = 3$  level of Fig. 2.1). Once these have been eliminated, we proceed by eliminating the second to last set of separator unknowns (e.g., those defined on  $\ell = 2$  in Fig. 2.1). The process continues eliminating unknowns associated with successively lower levels. This process can be viewed as an elimination tree, illustrated in Fig. 2.2.

The elimination tree indicates dependencies between operations. Each node is a cluster in the graph of  $A$  (separator or leaf-interior), and a cluster can only be eliminated once all its descendant have been eliminated. The clusters are then eliminated from bottom to top. This follows from the fact that eliminating a parent before a child would create edges between clusters previously separated, breaking the purpose of the ordering. ND is an ordering that limits fill-in: by eliminating clusters from bottom to top, one never creates edges (i.e., fill-in) between clusters previously separated.

The elimination procedure can also be represented in matrix form. Denote the total number of levels by  $L$  (where the leaves correspond to  $\ell = L$  and the root to  $\ell = 1$ ). Define  $A^{(L)}$  as the entire matrix and let  $A^\ell$  (for  $\ell < L$ ) be the Schur

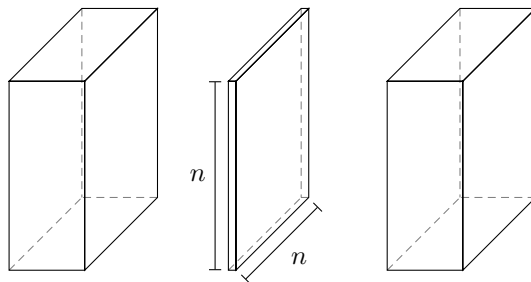


Fig. 2.3: Classical ND in 3D with  $N = n^3$  nodes: the top separator is of size  $\mathcal{O}(n^2)$ . Once the left and right clusters have been eliminated the top separator becomes completely dense, making its elimination alone cost  $\mathcal{O}((n^2)^3) = \mathcal{O}(N^2)$ .

complement operator (trailing matrix) obtained by eliminating levels  $\ell+1, \dots, L$ . The matrix obtained after eliminating the  $\ell+1$  level can be written in a block-arrowhead form

$$A^{(\ell)} = \begin{bmatrix} A_{11}^{(\ell)} & & & A_{1q}^{(\ell)} \\ & \ddots & & \vdots \\ & & A_{mm}^{(\ell)} & A_{mq}^{(\ell)} \\ A_{q1}^{(\ell)} & \dots & A_{qm}^{(\ell)} & A_{qq}^{(\ell)} \end{bmatrix}$$

where  $m = 2^{\ell-1}$  and  $q = m + 1$ . Here,  $A_{qq}^{(\ell)}$  refers to the matrix associated with all separators at levels  $1, \dots, \ell-1$ . The  $A_{ii}$  (for  $i \leq m$ ) are the matrices associated with non-eliminated unknowns within the  $i^{\text{th}}$  disconnected separators on the  $\ell^{\text{th}}$  level. The Schur complement can now be written as

$$A^{(\ell-1)} = A_{qq}^{(\ell)} - \sum_{i=1}^m A_{qi}^{\ell} (A_{ii}^{\ell})^{-1} A_{iq}^{\ell}.$$

This new matrix can then be interpreted as another block-arrowhead matrix associated with level  $\ell-1$  and so the elimination procedure can be repeated.

While limited, the fill-in is still significant. For instance, once all descendants of the top-separators have been eliminated, the top separator is typically completely filled (dense). For problems arising from the discretization of PDE's in 3D with  $\mathcal{O}(N) = \mathcal{O}(n^3)$  degrees of freedom (dofs), the top separator typically has size  $\mathcal{O}(N^{2/3}) = \mathcal{O}(n^2)$ . For instance in a regular  $n \times n \times n$  cube with  $N = n^3$  dofs and a 7-points stencil (or any other stencil with only “local” connections), the top separator is a plane (see Fig. 2.3) of size  $n \times n = n^2 = N^{2/3}$ . Hence, its factorization will cost  $\mathcal{O}(N^{2/3 \times 3}) = \mathcal{O}(N^2)$ , leading to quadratic or near-quadratic algorithms. While this is only formally valid on regular cubic-shaped graphs, the issue extends beyond those problems [39]: the separators in 3D graphs are typically very large, leading to large Schur complements and an expensive factorization, with complexity well above  $\mathcal{O}(N)$ .

Our algorithm addresses this specific concern by continually decreasing the size of all separators to keep fill-in to a minimum. It does so using low-rank approximations, and the factorization is then only approximate. In most cases under consideration, the separator size is typically decreased to  $\mathcal{O}(n) = \mathcal{O}(N^{1/3})$  so that its factorization costs  $\mathcal{O}(N)$ .

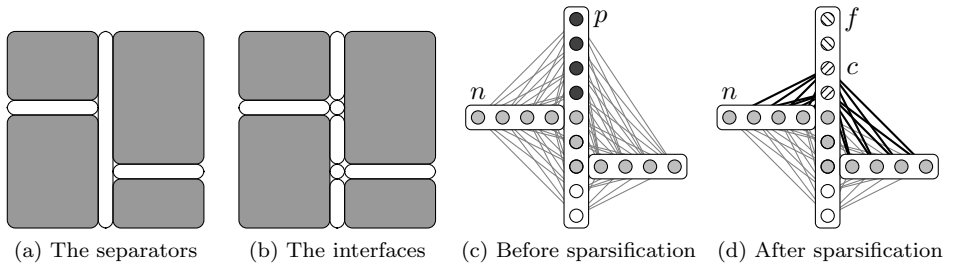


Fig. 2.4: Separator sparsification process. The first picture depicts the usual ND separator. The grey boxes have been eliminated. The second picture shows the different interfaces to be sparsified. The third and fourth picture focus on a given interface defined by  $p$  and connected to  $n$ . On the fourth picture, we have transformed  $p$  into  $f$  and  $c$  through a change of basis (not shown here) and up to a small  $\mathcal{O}(\varepsilon)$  error.  $f$  is now disconnected from both  $n$  and  $w$  and can be eliminated, without introducing any fill-in. Dark edges are edges updated by the sparsification.

**2.2. Sparsified Nested Dissection.** As noted, the sub-blocks created by the repeated Schur complement process become denser. To further limit fill-in, we introduce a sparsification algorithm that is invoked after all eliminations associated with a particular level have been performed. To motivate the sparsification, let us first consider a very simple case. Suppose we are about to eliminate level  $\ell$  and that there exist a subset of the  $j^{\text{th}}$  separator such that the corresponding rows in  $A_{jq}^{(\ell)}$  are relatively small. An inexact or incomplete factorization can be defined by simply ignoring these small rows. This effectively decouples those unknowns from the rest of the system so that they can be eliminated right away, without causing an increase in the number of non-zeros in the next recursive Schur complement. We can think of this as decreasing the size of the  $j^{\text{th}}$  separator. While  $A_{jq}^{(\ell)}$  will not generally have small rows, we instead seek a transformation that produces the desired small rows without altering the nonzero structure of the matrix. Further, this transformation will not only be applied to the off-diagonal blocks in the level  $\ell$  arrowhead matrix, but to all the non-eliminated degrees of freedom (dofs) (including those in  $A_{qq}^{(\ell)}$ ). This means we will effectively decrease the size of all remaining separators at levels  $1, \dots, \ell$ .

To understand the transformation, it is best to switch to a different block structure for the matrix. Specifically, consider the matrix

$$A^{(\ell)} = \begin{bmatrix} \hat{A}_{11}^{(\ell)} & \dots & \hat{A}_{1M}^{(\ell)} \\ \vdots & \ddots & \vdots \\ \hat{A}_{M1}^{(\ell)} & \dots & \hat{A}_{MM}^{(\ell)} \end{bmatrix}$$

This matrix is equivalent to  $A^{(\ell)}$ , the use of the *hat* accent symbol is only to emphasize the different block structure. Each  $\hat{A}_{ii}^{(\ell)}$  corresponds to the sub-matrix associated with an *interface* (instead of a separator). Specifically, an interface is defined as a *subset* of a separator for which the left and right neighbors correspond to a given pair of separators at level  $\ell$ . These  $M$  interfaces are subsets of all the separators associated with non-eliminated levels (i.e., levels  $k$  with  $k \leq \ell$ ). Notice that many of the  $\hat{A}_{ij}^{(\ell)}$  are

zero as only neighboring interfaces are coupled. Fig. 2.4 shows the distinction between ND separators (Fig. 2.4a) and interfaces (Fig. 2.4b). The top-level (root) separator has been cut into 5 pieces, each associated to a pair of left and right neighbors.

Fig. 2.4c and Fig. 2.4d illustrates a typical situation and the effect of the sparsification. Let  $p$  be a subset of a ND separator (in dark grey) at the interface between two interiors and  $n$  be all its neighbors (in light grey). The remaining nodes are disconnected from  $p$  and can be ignored for the purpose of this discussion. In this situation, the leaf-level interiors (dark grey clusters on Fig. 2.4a and Fig. 2.4b) have been eliminated and only higher-levels separators are left. The greyed edges represent connections between degrees of freedom. Notice that edges never cross separators.

Let  $\hat{A}_{pn}$  denotes all the edges from  $p$  to  $n$ . Assuming  $\hat{A}_{pp} = I$  (this is not a restriction, see subsection 2.5), we can then consider this sub-matrix of  $A^{(\ell)}$

$$\begin{bmatrix} I & \hat{A}_{pn} \\ \hat{A}_{np} & \hat{A}_{nn} \end{bmatrix}$$

Then, compute a low-rank approximation

$$\hat{A}_{pn} = \underbrace{\begin{bmatrix} Q_{pf} & Q_{pc} \end{bmatrix}}_Q \begin{bmatrix} W_{fn} \\ W_{cn} \end{bmatrix} \text{ with } \|W_{fn}\| = \mathcal{O}(\varepsilon)$$

and verify that

$$\begin{bmatrix} Q^\top & \\ & I \end{bmatrix} \begin{bmatrix} I_{pp} & \hat{A}_{pn} \\ \hat{A}_{np} & \hat{A}_{nn} \end{bmatrix} \begin{bmatrix} Q & \\ & I \end{bmatrix} = \begin{bmatrix} I_{ff} & & \mathcal{O}(\varepsilon) \\ & I_{cc} & W_{fn} \\ \mathcal{O}(\varepsilon) & W_{fn}^\top & \hat{A}_{nn} \end{bmatrix}$$

The matrix  $Q$  is a change of variables, transforming  $p$  into  $f$  (“fine”) and  $c$  (“coarse” — following AMG’s terminology, [49]). If we then ignore the  $\mathcal{O}(\varepsilon)$  edges, we have effectively decoupled the  $f$  variables from the rest, i.e., we have eliminated  $f$ . Notice that this didn’t create any fill-in:  $\hat{A}_{nn}$  is unchanged. As a result, we effectively *decreased the size of the separator*, without altering the nested dissection ordering. In the following, we will drop the hat notation, as it should be clear from the context whether we are referring to separators or interfaces.

The algorithm then alternate between classical “interiors” elimination (using a block Cholesky factorization) and “interfaces” sparsification as explained above. Fig. 2.5 illustrates the algorithm on a problem with 3 levels, where greyed boxes represent eliminated dofs at each level. Fig. 2.5a is the classical first step of a ND algorithm where we eliminate the leaf clusters (interiors at level 3). The second step in Fig. 2.5b is the sparsification step. We consider the interfaces between all the interiors (all the elongated ovals in Fig. 2.5a) and sparsify them, effectively reducing their size (Fig. 2.5b). Then the algorithm proceeds, alternating between interiors elimination and interfaces sparsification.

Algorithm 2.1 presents a high-level version of the algorithm. We name the algorithm spaND, referring to “sparsified Nested Dissection”.

The subsequent sections explain in detail the ordering & clustering (i.e., how we define the “interfaces”), the elimination and sparsification.

**2.3. Ordering and Clustering.** In addition to ordering, an appropriate clustering of the dofs has to be performed to define the various interfaces between interiors. That is, a simple ND ordering, by itself, does not give any indication about what the

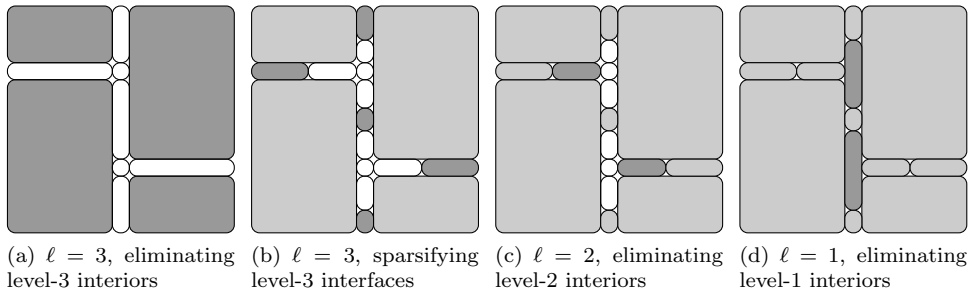


Fig. 2.5: Elimination & sparsification process. We start by eliminating all interiors (Fig. Fig. 2.5a) Then, all interfaces are sparsified (Fig. Fig. 2.5b) Dark grey clusters are nodes eliminated at a given step, light grey are previously eliminated nodes In practice, the sparsification introduces a change of variables, not depicted on this picture.

---

**Algorithm 2.1** High-level description of the spaND algorithm

---

**Require:** Sparse matrix  $A$ , SPD, Maximum level  $L$

Compute a ND ordering for  $A$ , infer interiors, separators and interfaces (see [subsection 2.3](#))

**for all**  $\ell = L, \dots, 1$  **do**

**for all**  $V_k^\ell$  interior **do**

    Eliminate  $V_k^\ell$  (see [subsection 2.4](#))

**end for**

**for all**  $W_p^\ell$  interface between separators **do**

    Sparsify  $W_p^\ell$  (see [subsection 2.5](#) and [subsection 2.6](#))

**end for**

**end for**

---

interfaces between different interiors are. To see this, consider [Fig. 2.1](#) (bottom row). This figure illustrates a classical ND ordering process. At every step, interiors are further separated by computing vertex separators. However, there is no clear way to define interfaces between interiors as shown on [Fig. 2.4](#) for instance. This cannot readily be calculated or even properly defined with a “usual” ND ordering.

To solve this issue, we have to keep track of the boundary of each interior during the ordering process. By then separating an interior *and* its boundary using vertex separators, we can keep track of the interfaces. [Fig. 2.6](#) illustrates this. Let  $V_k^{\ell-1}$  be the  $k^{\text{th}}$  interior (a cluster of dofs) at level  $\ell - 1$ . Let  $W_k^{\ell-1}$  be its boundary. We then perform a ND step on the graph induced by the *union* of those two sets,  $V_k^{\ell-1} \cup W_k^{\ell-1}$ . After this, we obtain the result on the right, where we now have two new interior (resp.  $V_{2k-1}^\ell$  and  $V_{2k}^\ell$ ) and boundary sets (resp.  $W_{2k-1}^\ell$  and  $W_{2k}^\ell$ ). Performing this operation recursively allows us to properly define and keep track of interiors and boundaries.

[Algorithm 2.2](#) is a modified ND algorithm that calculates interiors and interfaces. The only building block is a vertex-separator routine. From the sequence of  $V_k^{\ell}$ 's and  $W_k^{\ell}$ 's, one can infer the interiors at each level (for elimination) and the interfaces between each pair of interiors (for sparsification).

Each ND separator  $S_k^\ell$  is associated with a hierarchy of clusters with  $L - \ell + 1$ .



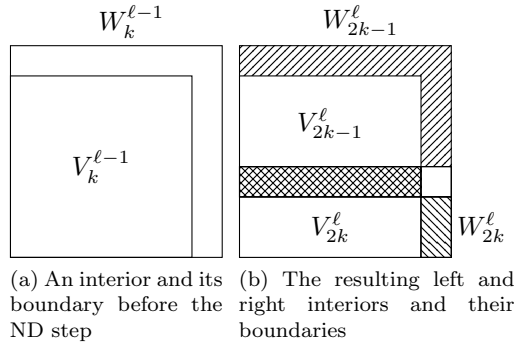


Fig. 2.6: The clustering & ordering building block. On the left, an initial interior and its boundary. On the right, the resulting separated interiors and boundaries, as well as the actual ND separator.

After  $\ell'$  levels of ND elimination, the separator  $S_k^\ell$  ( $\ell \geq \ell'$ ) is split into a number of clusters. These clusters can be defined by looking at all the subsets induced by the intersection of  $S_k^\ell$  and  $W_{k'}^{\ell'}$  for all  $k'$ .

Fig. 2.7 illustrates the process. On the top row, we illustrate the various  $\hat{S}_k^\ell$ , i.e., the separators of all interiors and interfaces. The important distinction with Fig. 2.1 is that the computed vertex-separators overlap with the boundaries to keep track of interfaces. On the middle row, we illustrate the actual clusters at each level and how the ND separators are broken into pieces. Separators at each level are depicted in a different color. We see that to each separator is associated a hierarchy of clusters. Finally, the bottom row shows such a hierarchy within each separator and how those have to be merged when going from a lower to higher level.

---

**Algorithm 2.2** Ordering & clustering algorithm.

---

**Require:**  $V$ , vertices,  $E$ , edges,  $L$  levels

$V_1^0 \leftarrow V$  {Interior}

$W_1^0 \leftarrow \emptyset$  {Boundary}

**for all**  $\ell = 1, \dots, L$  **do**

**for all**  $k = 1, \dots, 2^{\ell-1}$  **do**

$U \leftarrow V_k^{\ell-1} \cup W_k^{\ell-1}$

$(\hat{L}_k^\ell, \hat{S}_k^\ell, \hat{R}_k^\ell) = \text{vertex\_sep}(U, E|_U)$  {Computed vertex-separator}

$S_k^\ell \leftarrow \hat{S}_k^\ell \cap V_k^{\ell-1}$  {Actual Nested Dissection separator}

$V_{2k-1}^\ell, V_{2k}^\ell = \hat{L}_k^\ell \cap V_k^{\ell-1}, \hat{R}_k^\ell \cap V_k^{\ell-1}$  {Interiors at next level}

$W_{2k-1}^\ell, W_{2k}^\ell = \hat{L}_k^\ell \cap W_k^{\ell-1}, \hat{R}_k^\ell \cap W_k^{\ell-1}$  {Boundaries at next level}

**end for**

**end for**

---

**2.4. Separators Elimination using Block Cholesky.** Now that the matrix has been ordered and that dofs have been grouped into clusters defining various interfaces, the next step is to eliminate the interiors or separators at a given level  $\ell$  of the ND tree, as in a usual direct solver (see Algorithm 2.1). This section describes

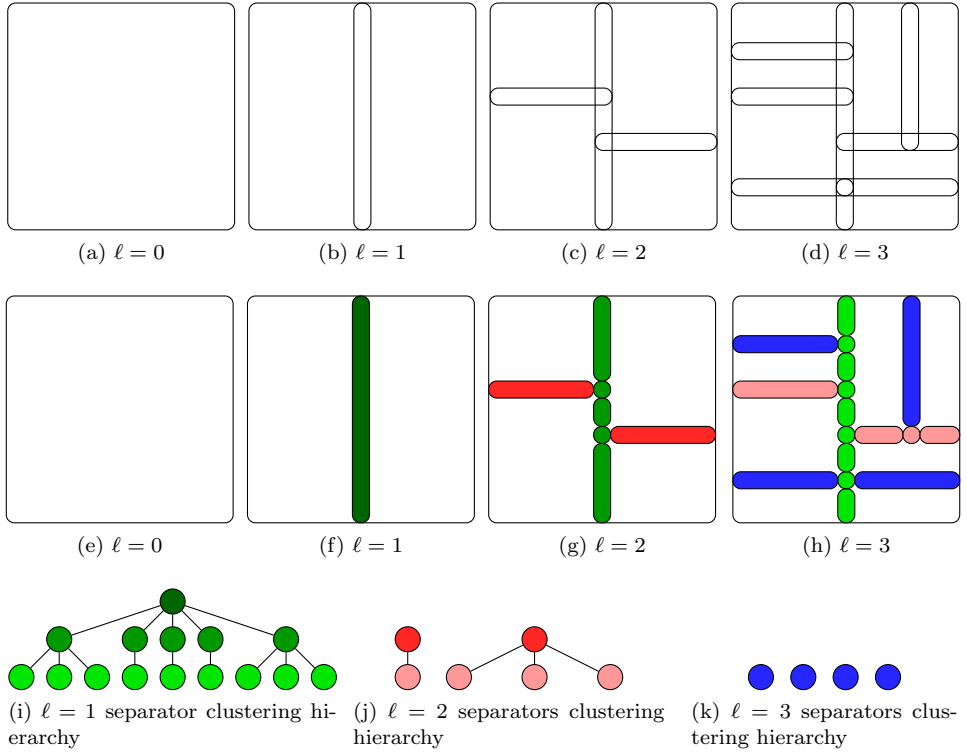


Fig. 2.7: A modified ND ordering & clustering (Algorithm 2.2). The top row indicates the separators  $\hat{S}_k^\ell$  computed at each step by separating interiors & boundaries. The middle row illustrates the clustering of dofs in each separator creating the interfaces between interiors. The bottom row shows the clusters hierarchy within each ND separator.

this elimination step, which is simply a standard block Cholesky reinterpreted with our notation. Consider  $A$  into the “block-arrowhead” form following the ND ordering

$$A = \begin{bmatrix} A_{ss} & & A_{sn} \\ & A_{ww} & A_{wn} \\ A_{ns} & A_{nw} & A_{nn} \end{bmatrix}$$

We indicate the separator or interior of interest by  $s$ , its neighbors by  $n$  and all disconnected nodes by  $w$ . By symmetry,  $A_{ab} = A_{ba}^\top$ .

Let  $L_s L_s^\top = A_{ss}$  the Cholesky factorization of  $A_{ss}$ . Then, define

$$E_s = \begin{bmatrix} L_s^{-1} & & \\ & I & \\ -A_{ns} A_{ss}^{-1} & & I \end{bmatrix}$$

Then, applying  $E_s$  on the left and right of  $A$  leads to

$$E_s A E_s^\top = \begin{bmatrix} I & & \\ & A_{ww} & A_{wn} \\ & A_{nw} & A_{nn} - A_{ns} A_{ss}^{-1} A_{sn} \end{bmatrix} = \begin{bmatrix} I & & \\ & A_{ww} & A_{wn} \\ & A_{nw} & B_{nn} \end{bmatrix}$$

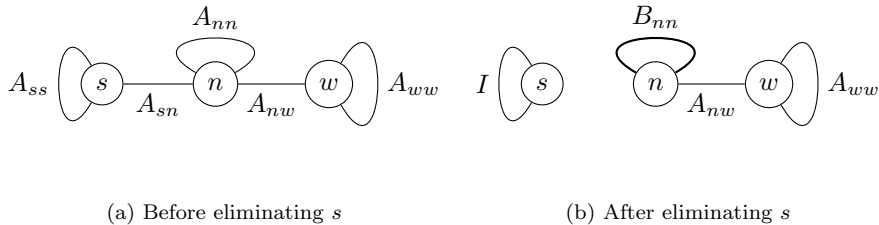


Fig. 2.8: Before and after the elimination of the separator  $s$  using block Cholesky. Eliminating  $s$  disconnects it from the rest, but requires updating the  $A_{nn}$  edges, connecting all neighbors  $n$  of  $s$

We notice that this may introduce (potentially many) new  $n_i-n_j$  edges not present before, a fill-in. However, there was no modification involving  $w$ . This is key in the ND ordering: there are no edges  $s-w$ , so no fill-in outside the neighbors.

Fig. 2.8 shows the elimination process from the matrix' graph perspective. We see that  $s$  is now isolated from the rest of the graph. We say that  $s$  has been *eliminated*. Furthermore, the effect on the *rest* of the graph was to update the self edge  $n-n$ ,  $A_{nn}$ . Separated nodes ( $w$ ) remain untouched.

**2.5. Interfaces Scaling.** Once that the separators or interiors at a given level have been eliminated, the algorithm goes through each interface and sparsifies it. However, a critical step before this is the proper scaling of each of those clusters. The goal is to scale (what is left of)  $A$  such that each diagonal block corresponding to a given interface is the identity. This provides theoretical guarantees (section 3) and significantly improves the accuracy of the preconditioner (section 4).

Consider the matrix

$$A = \begin{bmatrix} A_{pp} & A_{pn} \\ A_{np} & A_{nn} \end{bmatrix}$$

We define the block-scaling operation over  $p$  as

$$S_p = \begin{bmatrix} L_p^{-1} & \\ & I \end{bmatrix}$$

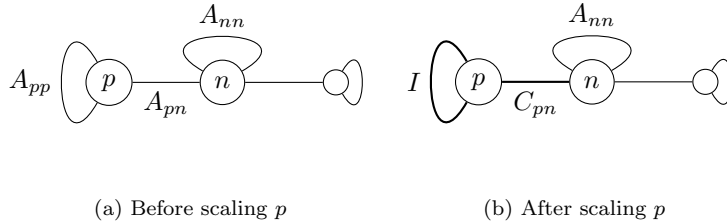
The result is

$$S_p A S_p^\top = \begin{bmatrix} I & L_p^{-1} A_{pn} \\ A_{np} L_p^{-\top} & A_{nn} \end{bmatrix} = \begin{bmatrix} I & C_{pn} \\ C_{np} & A_{nn} \end{bmatrix}$$

also depicted on Fig. 2.9. We see that a scaling of  $p$  requires modifying the edges involving  $p$  itself, but it has no other effect than that.

**2.6. Interface Sparsification using Low-Rank Approximations.** Now that interiors have been eliminated and each interface scaled, the final step is the sparsification. At this stage, the algorithm will go through each interface,  $p$ , and sparsify it, using low-rank approximations. Consider again

$$A = \begin{bmatrix} A_{pp} & A_{pn} \\ A_{np} & A_{nn} \end{bmatrix}$$

Fig. 2.9: Scaling of an interface  $p$ 

**2.6.1. Using orthogonal transformations.** Let us assume  $A_{pp} = I$ . This is not a loss of generality, as it can always be obtained by scaling  $p$ , as described in the previous section. Let us also assume that  $A_{pn}$  can be well approximated by a low-rank matrix, i.e.,

$$A_{pn} = Q_{pc}W_{cn} + Q_{pf}W_{fn}, \quad \|W_{fn}\|_2 = \mathcal{O}(\varepsilon)$$

where  $Q_{pc}$  is a thin orthogonal matrix and  $Q_{pf}$  its complement. This can be computed using a rank-revealing QR (RRQR) or a singular value decomposition (SVD) [26, 11, 29]. We use the letters  $c$  to denote the “coarse” (also known as “skeleton” or “relevant”, [36]) dofs, and  $f$  the “fine” (“redundant” or “irrelevant”) dofs. Let  $Q_{pp}$  be a square orthogonal matrix built as  $Q_{pp} = [Q_{pf} \quad Q_{pc}]$ . This implies

$$Q_{pc}^\top A_{pn} = W_{cn}, \quad Q_{pf}^\top A_{pn} = W_{fn} = \mathcal{O}(\varepsilon)$$

Then, define

$$(2.1) \quad Q_p = \begin{bmatrix} Q_{pp} & \\ & I \end{bmatrix}$$

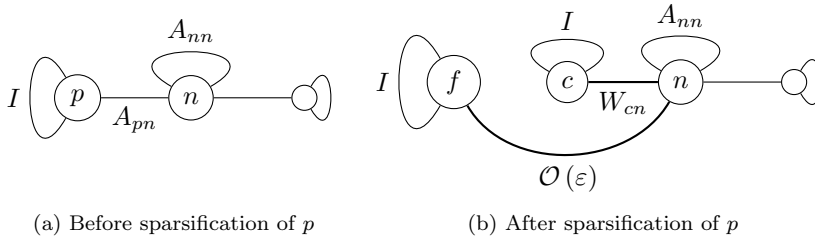
We see that

$$Q_p^\top A Q_p = \begin{bmatrix} I & & W_{fn} \\ & I & W_{cn} \\ W_{fn}^\top & W_{cn}^\top & A_{nn} \end{bmatrix} = \begin{bmatrix} I & & \mathcal{O}(\varepsilon) \\ & I & W_{cn} \\ \mathcal{O}(\varepsilon) & W_{cn}^\top & A_{nn} \end{bmatrix}$$

Fig. 2.10 shows the effect of the sparsification on the matrix graph. This is the key picture (compare with Fig. 2.4). We see that, after the orthogonal transformation,  $f$  only has very “weak” connections to  $n$ . If we ignore the  $\mathcal{O}(\varepsilon)$  term, this is the same as dropping the  $n$ – $f$  edge. This effectively means  $f$  has been eliminated.

However, note that this did *not* introduce any new edge with any of the neighbors of  $p$ . This is the key difference with a “regular” elimination as described previously: we can eliminate part of a cluster, here  $f$ , *without forming new edges between its neighbors*. The  $n$ – $n$  edge is unaffected by this operation (i.e., there is no fill-in). A regular elimination, on the other hand, would have changed the edges  $n$ – $n$ .

**2.6.2. Variant using Interpolative Transformations.** The previous section details the sparsification process using orthogonal transformations. However, this can also be done using other transformations. In this section we explain one variant using interpolative factorization, which was the original idea in [36].

Fig. 2.10: Sparsification of  $p$  using orthogonal transformation.

Assume we can *partition*  $p = c \cup f$  (so in this case  $c$  and  $f$  are subsets of  $p$ ) such that

$$A_{nf} = A_{nc}T_{cf} + \mathcal{O}(\varepsilon).$$

This is often called “interpolative decomposition”. It can be computed for instance using a rank-revealing QR (RRQR) factorization [18] (note that the RRQR is computed over  $A_{np}$  instead of  $A_{pn}$  in [subsubsection 2.6.1](#)): computing a RRQR over  $A_{np}$  leads to (with  $P$  the permutation, and  $R_{22} = \mathcal{O}(\varepsilon)$ )

$$\begin{aligned} [A_{nc} \quad A_{nf}] &= A_{np}P = [Q_1 \quad Q_2] \begin{bmatrix} R_{11} & R_{12} \\ & R_{22} \end{bmatrix} \\ \Rightarrow A_{nf} &= \underbrace{Q_1 R_{11}}_{A_{nc}} \underbrace{R_{11}^{-1} R_{12}}_{T_{cf}} + \underbrace{Q_2 R_{22}}_{=\mathcal{O}(\varepsilon)} \end{aligned}$$

Note that this factorization can also be computed using randomized methods [38]. This technique is referred to as “interpolative” because it is exact on  $A_{nc}$ : only  $A_{nf}$  is approximated and  $T_{cf}$  acts as an interpolation operator (i.e., as a set of Lagrange basis functions).

Now, consider

$$T_p = \begin{bmatrix} I & & \\ -T_{cf} & I & \\ & & I \end{bmatrix}$$

Notice how  $T_p$  is an upper-triangular matrix, while  $Q_p$  in [Eq. 2.1](#) was orthogonal. Both can be efficiently inverted ; however, working with orthogonal matrices bring stability guarantees (see [section 3](#)). Then,

$$T_p^\top A T_p = \begin{bmatrix} C_{ff} & C_{fc} & \mathcal{O}(\varepsilon) \\ C_{cf} & A_{cc} & A_{cn} \\ \mathcal{O}(\varepsilon) & A_{nc} & A_{nn} \end{bmatrix}$$

with

$$C_{ff} = A_{ff} - A_{fc}T_{cf} - T_{cf}^\top A_{cf} + T_{cf}^\top A_{cc}T_{cf}, \quad C_{cf} = A_{cf} - A_{cc}T_{cf}, \quad C_{fc} = C_{cf}^\top$$

[Fig. 2.11b](#) shows the matrix’ graph after the sparsification of  $p$  using interpolative factorization (and without prior scaling). Notice how  $f$  and  $c$  are still connected; however,  $f$  is (almost) disconnected from the rest of the matrix. We see that by ignoring

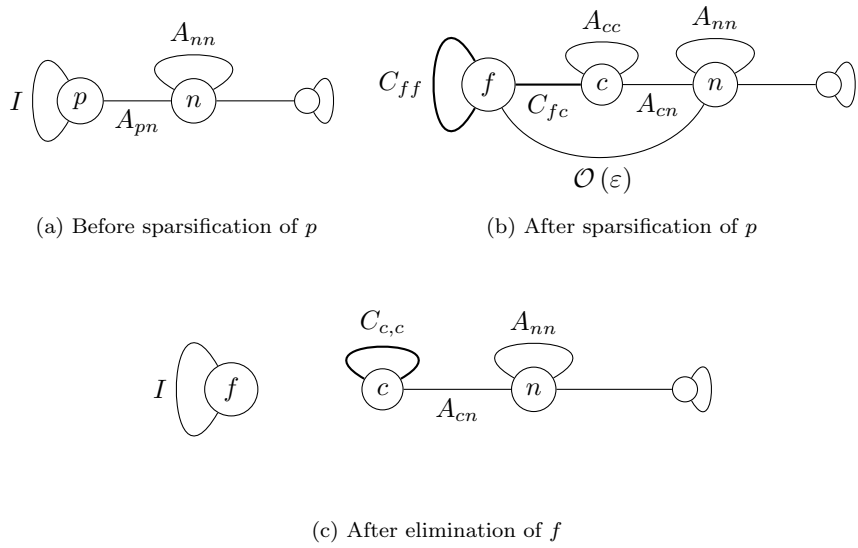


Fig. 2.11: Sparsification of  $p$  using interpolative factorization

the  $\mathcal{O}(\varepsilon)$  term, we can eliminate  $f$  immediately (with a classical block Cholesky, see [subsection 2.4](#)). The result is (note the updated  $c$ - $c$  edge) shown on [Fig. 2.11c](#).

The final result is the same as using orthogonal transformation. The differences are that

- $A_{pp}$  is not required to be identity;
- $A_{cn}$  is simply a subset of  $A_{pn}$ .

However, as we will see later on, there is a significant accuracy loss when using this technique without block scaling as opposed to orthogonal transformations with block scaling. Furthermore, it does not guarantee that the approximation stays SPD.

**2.7. Clusters merge.** Finally, once we have eliminated all separators at a given level, we need to merge the interfaces of every remaining ND separator. Consider for instance [Fig. 2.7](#). After having eliminated the leaf (level  $\ell = 4$ ) and the level  $\ell = 3$  separators, we need to merge the clusters in each separator. This is done following the cluster trees. Merging children clusters  $p_1, \dots, p_k$  into a parent cluster  $p$  simply means concatenating their dofs:

$$p = [p_1 \quad p_2 \quad \dots \quad p_k].$$

Then, all block rows and columns corresponding to  $p_1, \dots, p_k$  get concatenated into  $p$ .

**2.8. Sparsified Nested Dissection.** Now that we have introduced all the required building blocks (block elimination, scaling and sparsification), we can present the complete algorithm. Given a matrix  $A$ , appropriately ordered and clustered, the algorithm simply consists of applying a sequence of eliminations  $E_s$  ([subsection 2.4](#)), scalings  $S_p$  ([subsection 2.5](#)) and sparsification  $Q_p$  ([subsection 2.6](#)) (plus potentially some re-orderings and permutations to take care of the fine nodes  $f$  and the merge),

at each level  $\ell$ , effectively reducing  $A$  to (approximately)  $I$ :

$$M^\top AM \approx I \text{ with } M = \prod_{\ell=1}^L \left( \prod_{s \in S_\ell} E_s^\top \prod_{p \in C_\ell} S_p^\top \prod_{p \in C_\ell} Q_p \right)$$

In this expression,  $S_\ell$  are all the ND separators at level  $\ell$  and  $C_\ell$  are all the clusters (interfaces) in the graph right after level  $\ell$  elimination. Since  $M$  is given as a product of elementary transformations, it can easily be inverted. We refer to this algorithm as spaND, which stands for “sparsified Nested Dissection”. [Algorithm 2.3](#) presents the algorithm.

---

**Algorithm 2.3** The spaND algorithm (**OrthS**).

---

**Require:**  $A \succ 0$ ;  $L > 0$ ;  $\varepsilon$

$M = []$  (empty list)

Compute a  $L$ -levels modified ND ordering of  $A$  using [Algorithm 2.2](#). Infer clusters hierarchy in each ND separator.

**for all**  $\ell = L, \dots, 1$  **do**

**for all**  $s$  separator at level  $\ell$  **do** {Eliminate separators at level  $\ell$ }

    Eliminate  $s$ , get  $E_s$  ([subsection 2.4](#))

    Append  $E_s$  to  $M$

**end for**

**if**  $\ell < L$  **then**

**for all**  $s$  separator **do** {Merge clusters}

      Merge interfaces of  $s$  one level following clusters hierarchy ([subsection 2.7](#))

**end for**

**end if**

**for all**  $p$  interfaces **do** {Scale interface}

    Scale  $p$ , get  $S_p$  ([subsection 2.5](#))

    Append  $S_p$  to  $M$

**end for**

**for all**  $p$  interface **do** {Sparsify interfaces}

    Sparsify  $p$  with accuracy  $\varepsilon$ , get  $Q_p$  ([subsection 2.6](#))

    Append  $Q_p$  to  $M$

**end for**

**end for**

**return**  $M = \prod_{\ell=1}^L \left( \prod_{s \in S_\ell} E_s^\top \prod_{p \in C_\ell} S_p^\top \prod_{p \in C_\ell} Q_p \right)$  (such that  $M^\top AM \approx I$ )

---

We illustrate the effect of all the  $E_s$ ,  $S_p$  and  $Q_p^\top$  in  $A$  (i.e., the trailing matrix) on [Fig. 2.12](#). The two top rows show the actual trailing matrix, while the two bottom rows show the evolution of the matrix graph’s clusters as the elimination and sparsification proceeds.

**3. Theoretical results.** We here discuss a couple of facts related to the above factorizations.

**3.1. Sparsification and Error on the Schur Complement.** Consider a framework where

$$A = \begin{bmatrix} A_{pp} & A_{pn} \\ A_{np} & A_{nn} \end{bmatrix}.$$

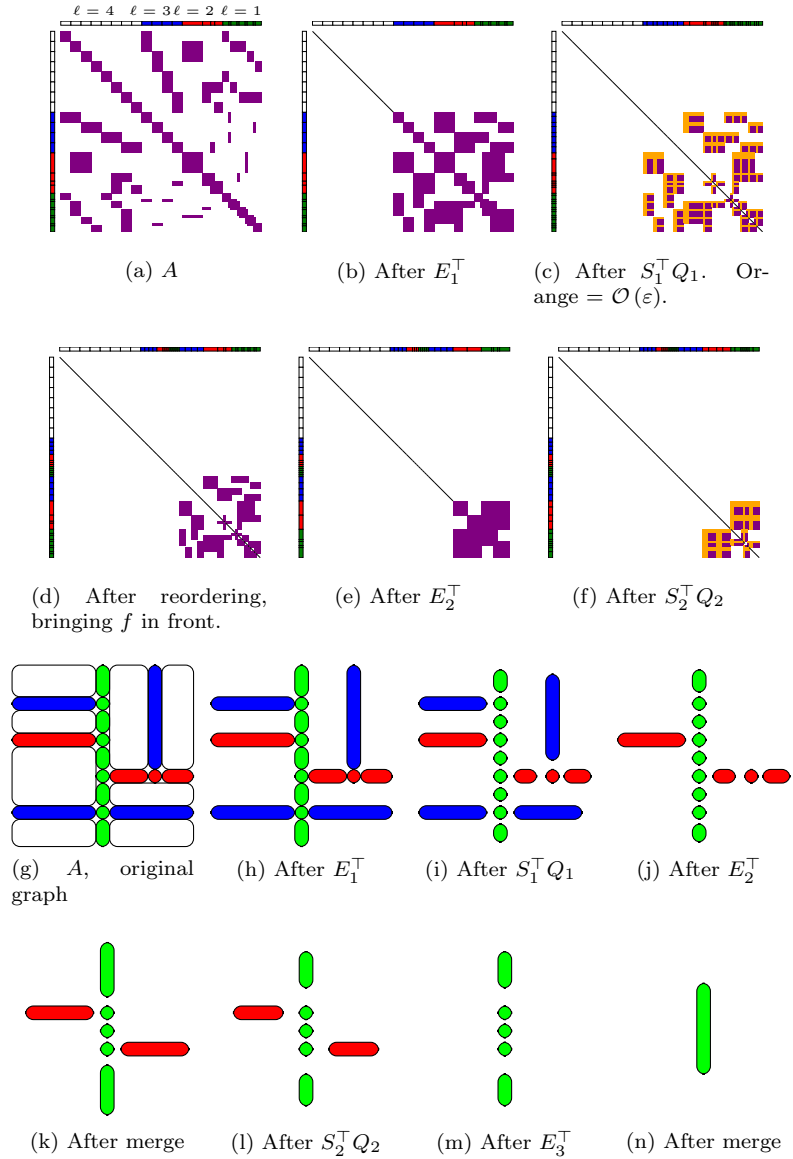


Fig. 2.12: Illustration of the spaND algorithm. Given  $A$ , create a ND tree of depth 4 and cluster  $A$  accordingly, as shown on Fig. 2.12g. This cartoon shows clusters of vertices of  $A$ , where the edges (not shown) should be thought as connecting close neighbors (like on a regular 2D grid). Denote by  $E_\ell$ ,  $S_\ell$  and  $Q_\ell$  all eliminations, scalings and sparsifications at level  $\ell$ . Then, we have  $E_4 E_3 (Q_2^\top S_2 E_2) (Q_1^\top S_1 E_1) A (E_1^\top S_1^\top Q_1) (E_2^\top S_2^\top Q_2) E_3^\top E_4^\top \approx I$ . The top rows show the evolution of the trailing matrix; bottom rows show the evolution of the matrix graph after eliminations, sparsifications and merges. We represent the sparsification process by shrinking the size of the clusters.



Without loss of generality, we do not include the  $w$ - $w$  and  $w$ - $n$  blocks, as they are completely disconnected from  $p$  and unaffected by the sparsification. Then, consider a general low-rank approximation

$$A_{pn} = X_1 Y_1^\top + X_2 Y_2^\top$$

where  $\|Y_2\| = \mathcal{O}(\epsilon)$ . Using  $X = [X_1 \ X_2]$  as a change of variable,  $A$  becomes

$$\begin{bmatrix} X^{-1} & \\ & I \end{bmatrix} \begin{bmatrix} A_{pp} & A_{pn} \\ A_{np} & A_{nn} \end{bmatrix} \begin{bmatrix} X^{-\top} & \\ & I \end{bmatrix} = \begin{bmatrix} B_{pp} & Y^\top \\ Y & A_{nn} \end{bmatrix} = \begin{bmatrix} B_{11} & B_{12} & Y_1^\top \\ B_{21} & B_{22} & Y_2^\top \\ Y_1 & Y_2 & A_{nn} \end{bmatrix}$$

The sparsification process then assumes  $Y_2 = 0$  and eliminates the 2-2 block. The true  $n$ - $n$  Schur complement is

$$S = A_{nn} - Y_2 B_{22}^{-1} Y_2^\top$$

while the approximate one, ignoring  $Y_2$ , is simply  $A_{nn}$ . The error is then

$$E_{nn} = Y_2 B_{22}^{-1} Y_2^\top.$$

We can now consider the different variants proposed in [subsection 2.6](#):

- (In) spaND using interpolative factorization and no diagonal block scaling. This gives  $B_{22} = C_{ff}$  and  $Y_2 = A_{nf} - A_{nc} T_{cf}$ , so that

$$\|E_{nn}\|_2 \leq \|Y_2\|_2^2 \|B_{22}^{-1}\|_2 = \mathcal{O}(\epsilon^2) \|C_{ff}^{-1}\|.$$

- (InS) spaND using interpolative factorization and diagonal block scaling. This leads to

$$\|E_{nn}\|_2 \leq \|Y_2\|_2^2 \|B_{22}^{-1}\|_2 = \mathcal{O}(\epsilon^2) \|C_{ff}^{-1}\|.$$

However, since  $A_{ss} = I$ ,  $C_{ff} = I + T_{cf}^\top T_{cf}$ , we can expect, if  $T_{cf}$  is small (which happens if the right algorithm is employed, see [\[40\]](#)),  $\|C_{ff}^{-1}\|$  to be much closer to 1.

- (OrthS) spaND using orthogonal factorization and diagonal block scaling. In this case, we simply have  $B_{22} = I$  and  $Y_2 = W_{fn}^\top$ , and so,

$$\|E_{nn}\|_2 \leq \|Y_2\|_2^2 = \mathcal{O}(\epsilon^2).$$

Table [3.1](#) summarizes the results. We notice that those three variants have roughly the same cost, since they requires a RRQR over  $A_{pn}$  or  $A_{np}$ , and their cost is proportional to  $\mathcal{O}(|p||n||c|)$  with  $|c|$  the resulting rank [\[26, Algorithm 5.4.1\]](#)

The key is that the interpolative error bound (without and to some extent with scaling) includes the potentially large  $\|C_{ff}^{-1}\|_2$  term, which is not present with the OrthS version. This indicates that we can expect the versions with diagonal scaling to have smaller errors  $E_{nn}$ . This will be verified in [section 4](#).

**3.2. Stability of the Block Scaling & Orthogonal Transformations Variant.** In addition to a smaller  $n$ - $n$  error as explained previously, the OrthS version provides stability guarantees.

**THEOREM 3.1.** *Let*

$$A = \begin{bmatrix} I & A_{pn} \\ A_{pn}^\top & A_{nn} \end{bmatrix}$$

Version	Error on $n-n$	Cost
In	$\mathcal{O}(\varepsilon^2) \ C_{ff}^{-1}\ _2$	$\mathcal{O}( p  n  c )$ $C_{ff}$ arbitrary
InS	$\mathcal{O}(\varepsilon^2) \ C_{ff}^{-1}\ _2$	$\mathcal{O}( p  n  c )$ $C_{ff} = I + T_{cf}^\top T_{cf}$
OrthS	$\mathcal{O}(\varepsilon^2)$	$\mathcal{O}( p  n  c )$

Table 3.1: Error for various approximations. The left column indicate the sparsification variant: **In** means interpolative and no scaling; **InS** means interpolative and scaling; **OrthS** means orthogonal and scaling.

be a SPD matrix. For any low-rank approximation

$$A_{pn} = Q_{pf}W_{fn} + Q_{pc}W_{cn}$$

where  $Q_p = [Q_{pf} \quad Q_{pc}]$  is a square orthogonal matrix

$$B_p = \begin{bmatrix} I & W_{cn} \\ W_{cn}^\top & A_{nn} \end{bmatrix}$$

is SPD.

*Proof.* The  $n-n$  Schur Complement of  $B_p$  (when eliminating  $c$ ) is

$$S_B = A_{nn} - W_{cn}^\top W_{cn}.$$

On the other hand, the  $n-n$  Schur Complement of  $A$  (when eliminating  $p$ ) is

$$S_A = A_{nn} - A_{np}^\top A_{pn} = A_{nn} - W_{cn}^\top W_{cn} - W_{fn}^\top W_{fn}$$

which implies

$$S_B = S_A + W_{fn}^\top W_{fn}.$$

Since  $A$  is SPD, so is  $S_A$ , and since  $W_{fn}^\top W_{fn} \succeq 0$ , we find that  $S_B$  is SPD. Since the  $c-c$  bloc of  $B_p$  is identity, we conclude that  $B_p$  is SPD.  $\square$

**COROLLARY 3.2.** *For any SPD matrix and  $\varepsilon \geq 0$ , the sparsified matrices of the spaND algorithm using block diagonal scaling and orthogonal low-rank approximations (**OrthS**) remain SPD. In other words, the algorithm never breaks down.*

Note that the above corollary does *not* depend on the quality of the low-rank approximation, i.e., it works even for  $\varepsilon = 0$ . It merely relies on the fact that the truncated error ( $Q_{pf}W_{fn}$ ) is orthogonal to what is retained ( $Q_{pc}W_{cn}$ ) and that the scheme is using a “weak admissibility” criterion (*all* edges of  $p$  are compressed). Finally, note that the above proof also shows that

$$S_B = S_A + \mathcal{O}(\varepsilon^2), \quad S_B \succeq S_A.$$

This is a classical result in the case of low-rank approximation using weak admissibility (see [56, 57] for instance).

**4. Numerical Experiments.** This section presents applications of the algorithm on various problems. All matrices are symmetric, real and positive-definite.

We use the following notation throughout this section:

- $t_F$  is the factorization time (in seconds), including partitioning;
- $t_S$  is the time (in seconds) required for CG to reach a relative residual of  $10^{-12}$ . While this is quite a small values, begin able to reach those tolerances is a good indication of the numerical stability of the algorithm (i.e., that the preconditioner does not prevent CG from converging to a small tolerance);
- $n_{CG}$  is the associated number of CG steps;
- $\text{size}_{\text{Top}}$  is the size of the top-separator right before elimination;
- $\text{mem}_F$  is the number of non-zero entries in the factorization;

On top of this, at some point we compare spaND to classical “exact” ND (using spaND with no compression & scaling; “Direct”) and to a classical ILU(0) [45] (“ILU(0)”).

All tests were run on a machine with 128 GO of RAM and a Intel(R) Xeon(R) CPU E5-2650 v2 2.60GHz. The algorithm is sequential and was coded in C++. We use the Intel(R) Compiler 2018 and Intel(R) MKL 2018 Update 1 for Linux for the BLAS & LAPACK operations. When no geometry information is available, we use Metis 5.1 [37] for the vertex-separator routine. We use Ifpack2 [43] for ILU(0). Low-rank approximations are performed using LAPACK’s geqp3 [4]. The truncation uses a simple rule, truncating based on the absolute value of the diagonal entries of the  $R$  factor. This means that, given  $R$ , we select the first  $r$  rows, where  $\frac{|R_{ii}|}{|R_{11}|} \geq \varepsilon$  for  $1 \leq i \leq r$ .

**4.1. Impact of Diagonal Scaling & Orthogonal Transformations.** In this first set of experiments we compare, empirically, the three variants of the algorithm:

- (In) spaND using interpolative factorization and no diagonal block scaling;
- (InS) spaND using interpolative factorization and diagonal block scaling;
- (OrthS) spaND using orthogonal factorization and diagonal block scaling.

This should be contrasted with prior work [36] where the algorithm was using the interpolative only variant (with no scaling).

**4.1.1. High-contrast 2D Laplacians.** We first consider 2D elliptic equations

$$(4.1) \quad \nabla(a(x) \cdot \nabla u(x)) = f \quad \forall x \in \Omega = [0, 1]^2, \quad u|_{\partial\Omega} = 0$$

where  $a(x)$  is a quantized high-contrast field with high of  $\rho$  and low of  $\rho^{-1}$  and where 4.1 is discretized with a 5-points stencil. This lead to the following discretization

$$(a_{i-1/2,j} + a_{i+1/2,j} + a_{i,j-1/2} + a_{i,j+1/2})u_{ij} - a_{i-1/2,j}u_{i-1,j} - a_{i+1/2,j}u_{i+1,j} - a_{i,j-1/2}u_{i,j-1} - a_{i,j+1/2}u_{i,j+1} = h^2 f_{ij}$$

The field  $a$  is built in the following way:

- create a random  $(0, 1)$  array  $\hat{a}_{ij}$ ;
- smooth  $\hat{a}$  by convolving it with a unit-width Gaussian;
- quantize  $\hat{a}$

$$a_{ij} = \begin{cases} \rho & \text{if } \hat{a}_{ij} \geq 0.5 \\ \rho^{-1} & \text{else} \end{cases}$$

Fig. 4.1 gives an example of high-contrast field for  $n = 32$  and  $n = 128$ .

We compare the number of iterations CG [35] needs to reach a residual of  $10^{-12}$ . In all those experiments, a missing value indicates the factorization was not SPD and, at some point, Cholesky (subsection 2.4) failed. Given that the problem is defined

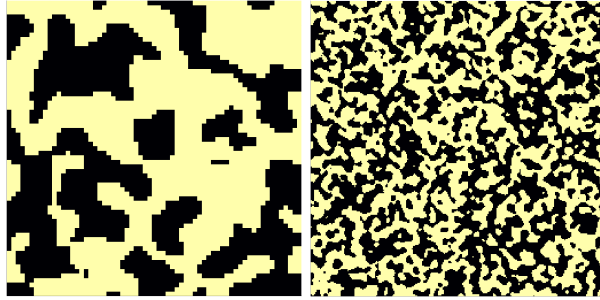


Fig. 4.1: A quantized high-contrast field with lows of  $\rho^{-1}$  and highs of  $\rho$  for  $n = 32$  (left) and  $n = 128$  (right). The features size are roughly constant as we increase the mesh size  $n$ .

on a regular mesh, we use a variant of [Algorithm 2.2](#) where the vertex-separator used is based on geometry. This leads to a more regular clustering and, in general, to slightly better performances (in terms of time or memory — CG iterations and the preconditioner accuracy are usually unaffected).

[Fig. 4.2](#) gives results for  $\rho = 1$  to  $\rho = 1000$ . We compare the three variants for various  $\varepsilon$  and problem size  $N = n^2$ . We observe three things from the experiment. First, the number of iterations, particularly at moderate accuracies ( $\varepsilon = 10^{-1}$  or  $10^{-2}$ ), is greatly reduced using `InS`. Further, the `OrthS` variant is usually the most accurate. This is likely due to the improved robustness and accuracies of the orthogonal transformations versus the interpolative ones. Finally, we see that, while the `In` and `InS` variants may fail due to non-SPD approximations, the `OrthS` never fails and can always be run, even at  $\varepsilon \approx 1$ . We finally note that the small target residual of  $10^{-12}$  in CG illustrates the good numerical properties of the preconditioner. Previous work [\[36\]](#) was focused on the interpolative only variant. Both the scaling and orthogonal transformations greatly improve the algorithm: they reduce the CG iteration count and guarantee that the preconditioner stays SPD for SPD problems.

**4.1.2. Non-Regular Problems.** [Fig. 4.3](#) gives results for three variants on all the SPD (real & square) problems from the SuiteSparse matrix collection [\[20\]](#) with more than 50 000 rows and columns. Most of these problems come from PDE discretization, but not all. `G2circuit` for instance comes from a circuit simulation problem and `finan512` comes from a portfolio optimization problem.

We see the algorithm converges for all problems. For most problems, an accuracy of  $\varepsilon = 10^{-2}$  leads to a number of iterations usually less than 100, while an accuracy of  $\varepsilon = 10^{-4}$  leads usually to less than 10 iterations. Only the `Botonakis/thermomech_TK` problem needs more than 100 iterations for  $\varepsilon = 10^{-6}$ .

[Fig. 4.4](#) shows a performance profile regarding the CG iteration count. Each plot compares the three variants for a given accuracy. For a given problem  $p$  and a variant  $v$ , let  $CG_{p,v}$  be the CG count and  $CG_p^*$  the best result among the three variants, for a problem  $p$ . Then each curve is defined as

$$T_v(t) = \frac{\#\left\{p \in P \mid \frac{CG_{p,v}}{CG_p^*} \leq t\right\}}{\#P}$$

Each value  $T_v(t)$  basically represent the fraction of problems where variant  $v$  is within

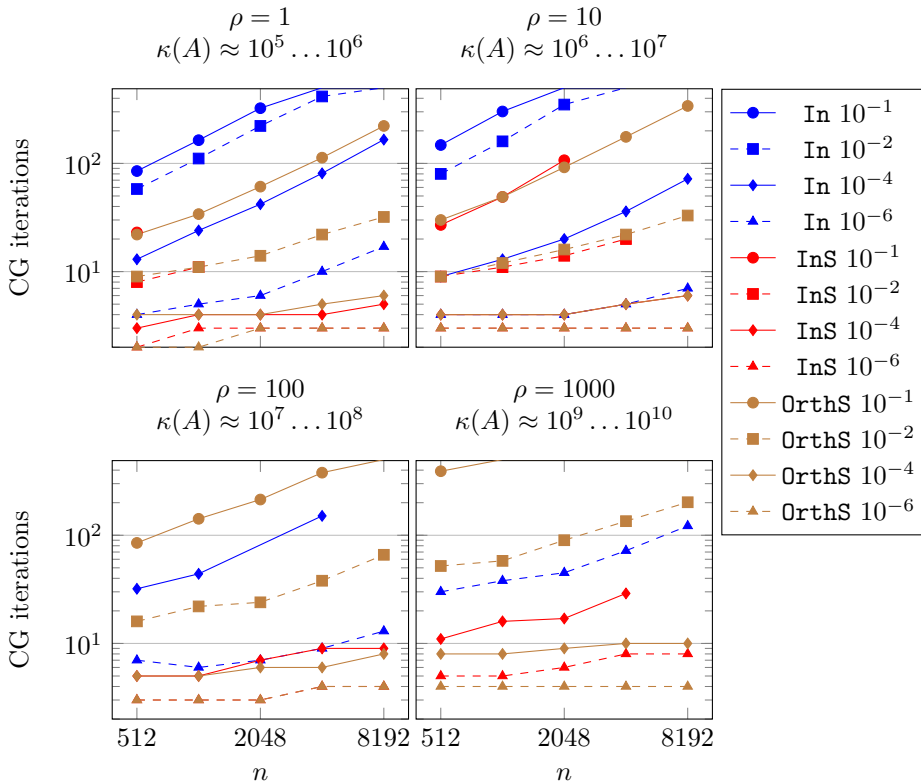


Fig. 4.2: 2D  $n \times n$  Laplacians: each line represent a given variant: **In** (interpolative and no scaling), **InS** (interpolative and scaling) and **OrthS** (orthogonal and scaling), at a given accuracy  $\varepsilon$ , from  $10^{-1}$  to  $10^{-6}$ . Each dot gives the CG iteration count, and we run the experiments on various problem of size  $N = n^2$ , for various  $\rho$ . The conditioning is roughly proportional to  $\rho$ . A missing data point means Cholesky broke down and the preconditioner is not SPD. This shows that, in general, **InS** and **OrthS** are much more accurate than **In** at a given accuracy. In addition, for small enough  $\varepsilon$ , the accuracy is roughly independent from the problem size  $N$ . Finally, when  $\rho$  is not too extreme, there is little dependency with the condition number.

$t$  times the best algorithm. The most interesting plots are  $\varepsilon = 10^{-2}$  and  $\varepsilon = 10^{-4}$ . On these, we see that the scaling has a drastic effect on the CG count. On  $\varepsilon = 10^{-1}$ , many cases do not converge (in under 500 iterations), so they have similar performances. Finally, on  $\varepsilon = 10^{-6}$ , most cases converge in a couples iterations, so the three variants have similar performances. The plots clearly shows that **OrthS** is the optimal strategy, being within at most 2 of the optimal in the worst case, and being often the winning algorithm.

Further, using orthogonal transformations guarantees that the approximation stays SPD, allowing the algorithm to not break down even for high  $\varepsilon$ 's. The number of iterations of **OrthS** is not always strictly smaller than the **InS** variant, while it is for the regular Laplacian examples. However, the extra robustness (no need for pivoting) of the orthogonal transformations make them quite attractive in practice

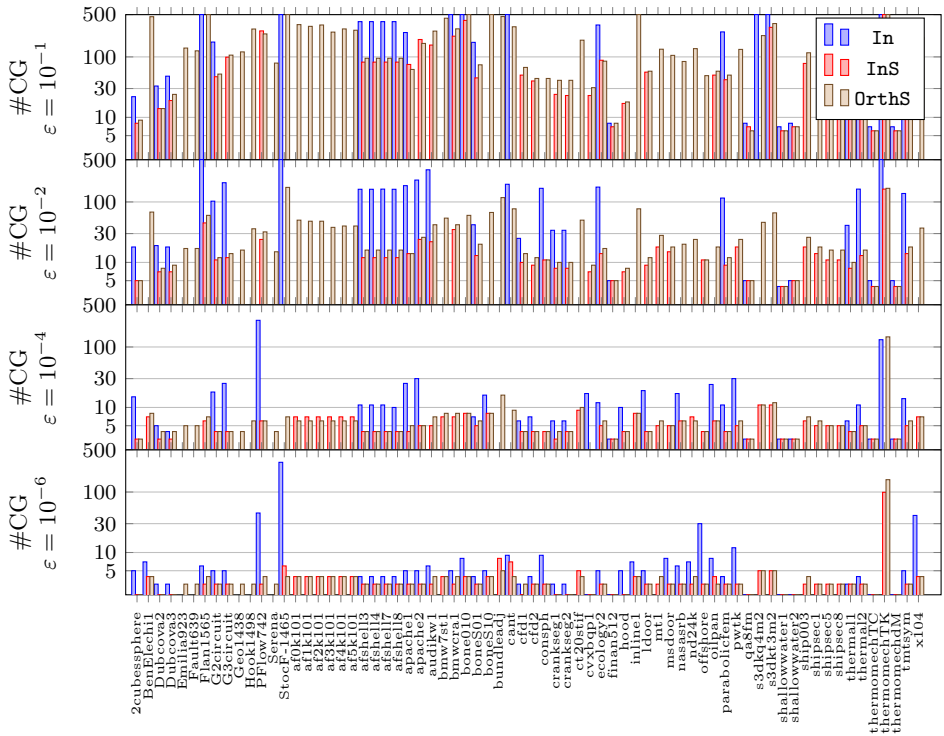


Fig. 4.3: SuiteSparse matrix collection: result on all the (real) SPD problems of the SuiteSparse matrix collections where  $N \geq 50\,000$ . The partitioning is only graph-based. Each bar represents the number of CG iterations for a given problem with a given variant of the algorithm: **In** (interpolative and no scaling), **InS** (interpolative and scaling) and **OrthS** (orthogonal and scaling) at a given accuracy  $\varepsilon$ . This shows that, as  $\varepsilon \rightarrow 0$ , the algorithm converges on a wide range of problems. This also shows that the scaling is beneficial in almost all cases. The orthogonal transformations, while not always better (in terms of accuracy) than the interpolative transformations, do guarantee that the preconditioner stays SPD and the factorization never breaks down because of indefinite pivots.

for SPD problems.

We also point out that previous work [36] was restricted to standard elliptic model problems. To the best of our knowledge, this is the first application of this algorithm to a wide range of problems.

**4.2. Scalings with problem size.** We now consider scalings, i.e., how does the algorithm perform as  $N$  grows. Fig. 4.5 shows the evolution of the top-separator size right before elimination (top) and the number of CG iterations (bottom) for  $\rho = 1$  and  $\rho = 100$  for  $3D$  problems generated as in subsection 4.1.1 with a classic 7-points stencil. For now on, we will only consider the scaling & orthogonal method (**OrthS**). This figure shows two properties of the algorithm:

- The top-separator size ( $\text{size}_{\text{Top}}$ ) typically grows like  $\mathcal{O}(N^{1/3})$ , regardless of  $\varepsilon$ ;

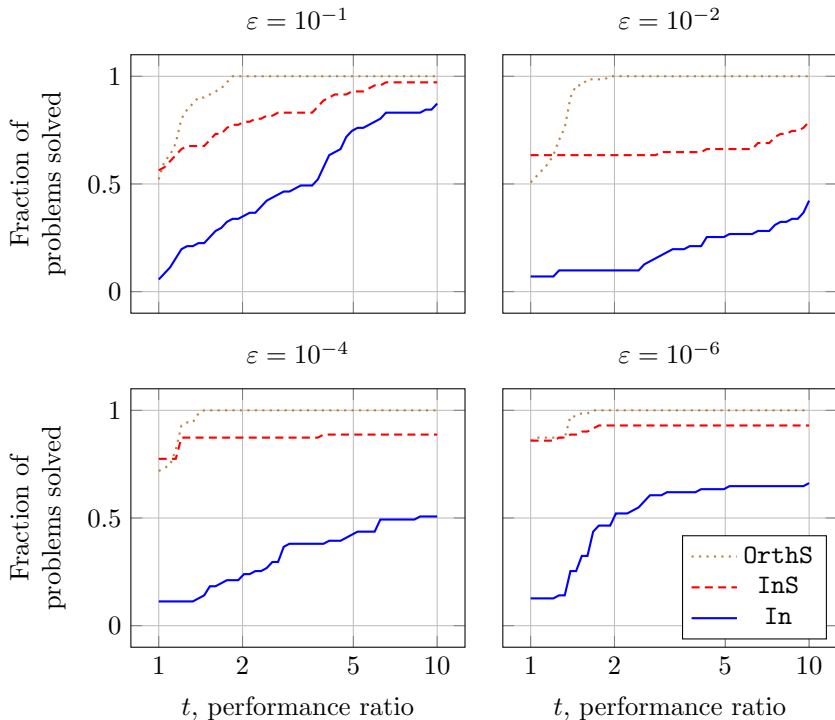


Fig. 4.4: Performance profile for all the SuiteSparse experiments (Fig. 4.3), where the performance criterion is  $\#CG$ , the number of CG iterations. Each point  $T_v(t)$  gives the fraction of problems for which variant  $v$  completed with a running time less than  $t$  times the best variant. An excellent method is one that starts at  $t = 1$  close to 1 and quickly reaches 1 as  $t$  increases. This means that this method outperforms the other methods in almost all cases. **InS** and **OrthS** typically have the same number of iterations, but **InS** sometimes leads to a non-SPD preconditionner, hence the difference in performances. **In** typically leads to a much larger iteration count. Looking at the bottom left figure ( $\varepsilon = 10^{-4}$ ) for example, we see that for half of the problems **In** has a cost more than 10 times greater than the best variant. For all cases, the **OrthS** is within a factor of 2 of the optimal CG iteration count. This shows the importance of the scaling.

- For small enough  $\varepsilon$ , the number of CG iterations is roughly  $\mathcal{O}(1)$ .

Combining those two properties, we can expect, for small enough  $\varepsilon$ ,

- a factorization time of  $\mathcal{O}(N^{1/3 \cdot 3}) = \mathcal{O}(N)$ ;
- a solve time of  $\mathcal{O}(N \cdot 1) = \mathcal{O}(N)$ ,

which implies that the algorithm scales roughly linearly with  $N$ . We do not formally prove those results (see [36] for a proof sketch).

**4.3. Timings and Memory Usage.** We now study the efficiency of the algorithm in terms of time (factorization and solve time) and memory usage on “real-life” problems. To evaluate our algorithm, we use the following two metrics:

- the factorization and solve time ( $t_F$  and  $t_S$ );
- the memory footprint ( $\text{mem}_F$ , the number of non-zeroes in the preconditioner

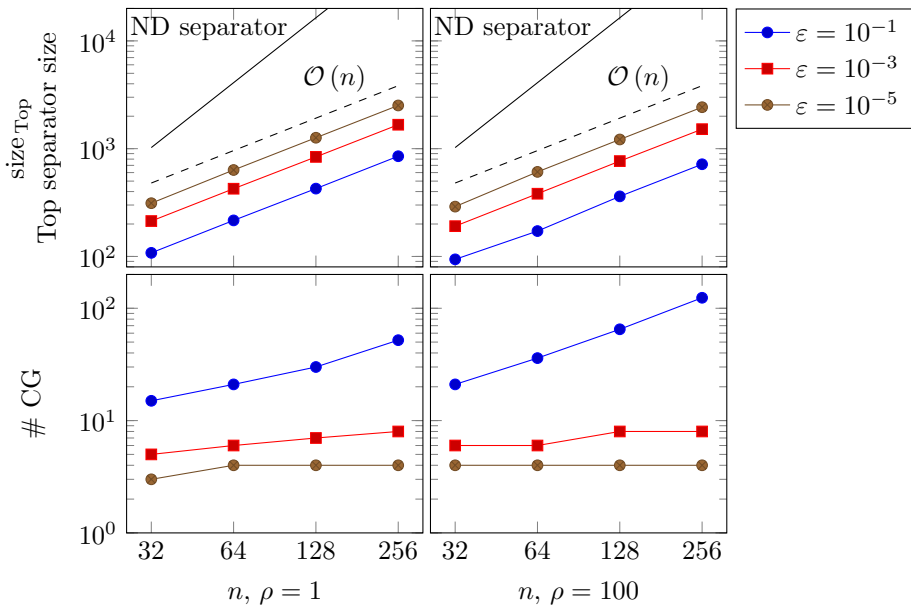


Fig. 4.5: 3D  $n \times n \times n$  Laplacian results for  $\rho = 1$  (left) and  $\rho = 100$  (right) using `OrthS`. We see that  $\text{size}_{\text{Top}}$  (top-separator final size, i.e., right before elimination) scales like  $\mathcal{O}(n)$ , and that increasing the accuracy (decreasing  $\varepsilon$ ) essentially adds a constant; it does not change the scaling. This should be compared with the classical ND separator size (solid like), equal to  $n^2$ . In addition, for a small enough  $\varepsilon$ , the CG iteration count becomes virtually constant. Both those fact mean the algorithm can be expected to have complexity  $\mathcal{O}(N)$ .

$M$ ).

*SuiteSparse.* Table 4.1 shows the results on two specific problems from the SuiteSparse collection [20], `inline` and `audikw`. For both problems, we see that the “sweet-spot” in terms of minimal time-to-solution is not for high  $\varepsilon$ , but for much smaller  $\varepsilon$ . For the `audikw` problem, the optimal is when using  $\varepsilon = 10^{-2}$ , and for `inline`,  $10^{-4}$  gives optimal result. The  $\text{size}_{\text{Top}}$  for `inline` are overall much smaller than for `audikw`. This is usually an indication that the problem is near 2D, for which  $\text{size}_{\text{Top}}$  is typically  $\mathcal{O}(1)$ . Those problems are of fairly small size and, as such, direct solvers (with smaller constants and better implementations) remain competitive.

*Ice-sheet modeling problem.* Table 4.2 gives the result on an ice-sheet modeling problem [50]. This problem comes from the modeling of ice flows on Antarctica using a finite-element discretization. The problem is challenging because of the high variations in background field and the near-singular blocks in the matrix, leading to a condition number of more than  $10^{11}$ . This problem is nearly 2D. The graph in the  $x, y$  plane is regular but non-square. It is then extruded in the  $z$  direction.

We illustrate the partitioning (top-left) and one layer of the solution (top-right, with a random right-hand side) on a log scale. Note the high variations in scales in the solution. This makes the problem very ill conditioned and hard to solve with classical preconditioners. Since the problem is (nearly) 2D and we are given the geometry, we partition the matrix in the  $xy$  plane and extrude the partitioning in the  $z$  direction.



Problem	$N$	$\varepsilon$	$t_F$ (s.)	$t_S$ (s.)	$n_{CG}$	$size_{Top}$	$mem_F$ ( $10^9$ )
audikw_1	943 695	$10^{-1}$	139	432	268	326	0.53
		$10^{-2}$	352	88	41	606	0.811
		$10^{-4}$	649	22	6	1175	1.23
inline_1	503 712	$10^{-1}$	52	214	> 500	2	0.12
		$10^{-2}$	55	38	82	13	0.14
		$10^{-4}$	61	4	7	19	0.17

Table 4.1: Some SuiteSparse performance results using `OrthS`. Completely general partitioning (no geometry information used). We see that the algorithm do converge when  $\varepsilon \rightarrow 0$ . The sweet spot varies for both problems. Notice that `inline_1` has a very small  $size_{Top}$ , characteristic of near-2D problems, which the top-separator has a much larger size for `audikw_1`.

The partitioning uses a classical recursive coordinate bisection approach [8].

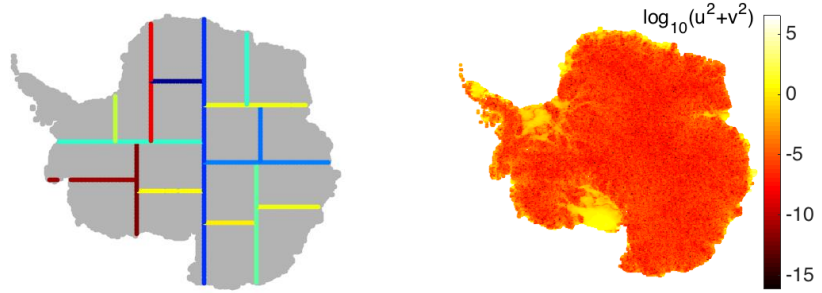
We use two sequences of matrices with a different number of layers in the  $z$  direction. We see that  $size_{Top}$  grows very slowly, close (but not exactly) like  $\mathcal{O}(1)$  for each set of problems. This is typical of 2D or near-2D problems. The memory use is roughly linear for each set of problems, and the factorization time is growing almost linearly. This validates the effectiveness of the algorithm.

We also compared the algorithm against a direct method (simply using `spaND` with no compression but otherwise with the same parameters). The results are in the “Direct” column. We note the very poor scaling of the direct method; our algorithm, on the other hand, performs much better. In addition, we also compared the algorithm to out-of-the-box algebraic multigrid (AMG, a classical AMG) and Incomplete LU(0). On this specific problem, AMG simply did not converge in less than 500 iterations, the residual stalling around 1.0. While specifically designed AMG can and does solve this problem well [50], this illustrates that out-of-box algorithms cannot always efficiently solve very ill-conditioned problems. Because of this, we do not report those results. We finally tested `Ifpack2`’s ILU(0) [43] with GMRES. We tested two ordering, horizontal (layer-wise) and vertical (column-wise). The layer-wise ordering gave (by far) the best performances and we report only this one. However, while it is competitive for small problems, it cannot solve large problems because the number of iterations grows quickly, making the algorithm too expensive. This illustrate the strong advantage of `spaND`: with a nearly constant number of iterations, we do not suffer from this deterioration of the preconditioner and can solve larger problems.

We note that those results can also be compared with recent work using `LoRaSp` [42, 17] on the same matrices. Overall, while the scaling with  $N$  is similar, `spaND` exhibits better constants.

*SPE benchmark.* Table 4.3 gives the results on a cubic slide of the SPE (Society of Petroleum Engineering) benchmark [19], a classical benchmark to evaluate oil & gas exploration codes. This matrix models a porous media flow. This problem is particularly challenging for direct methods since it resembles a 3D cubic problem and lead to a high complexity. On the other hand, it can be solved quite efficiently with classical preconditioners like AMG or ILU.

We use various values of  $n$ , and the problem is then of size  $N = n^3$ . The bottom pictures shows the  $size_{Top}$  and  $mem_F$  scaling with  $N$ . We see that  $size_{Top}$  grows roughly like  $\mathcal{O}(N^{1/3})$ ; this is typical of 3D problems. The memory use grows linearly



$N$	spaND					Direct	ILU(0)
	$t_F$ (s.)	$t_S$ (s.)	nCG	size <sub>TOP</sub>	mem <sub>F</sub> ( $10^9$ )	$t_F + t_S$ (s.)	$t_S$ (nGMRES) (s.)
5 layers							
629 544 (16 km)	6	3	7	78	0.15	22	23 (92)
2 521 872 (8 km)	27	15	8	88	0.63	206	290 (182)
10 096 080 (4 km)	180	101	10	99	2.61	1578	7571 (720)
10 layers							
1 154 164 (16 km)	24	7	8	137	0.42	90	50 (93)
4 623 432 (8 km)	104	37	8	147	1.73	710	550 (180)
18 509 480 (4 km)	758	322	10	159	7.59	—	15390 (745)

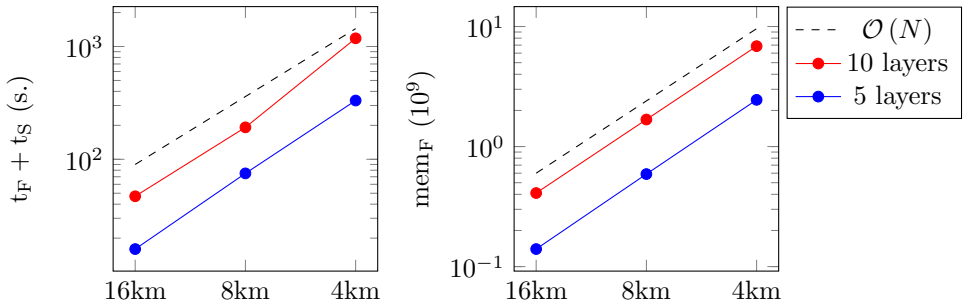
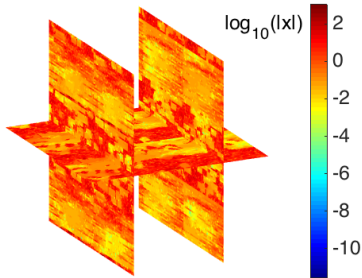


Table 4.2: Ice Sheet results. Unregular geometric partitioning,  $\varepsilon = 10^{-2}$ , `OrthS`. The top left picture illustrates the separators (for the top 5 levels) and the top right picture shows the solution (for a random right-hand side  $b$ ) on log scale. — indicates the algorithm ran out of memory. We run ILU with 2 ordering: layer-wise ordering and vertical column-wise ordering. The later lead to very poor convergence and is not shown here. This problem is very ill-conditioned and typically very hard to solve using out-of-the-box preconditioners. spaND, on the other hand, solves the problem well and scale near-linearly with the problem size.

with  $N$ . Furthermore, the number of CG iterations is constant for all resolutions. This serves as another validation of the ability of spaND to solve large-scale problems. In the last column, we show the result using the direct solver. Since it is a direct solver, the memory use is too significant, and we cannot solve the 4M problem. Furthermore, the time to solve the 2M problem is about 10 times more than using spaND. This shows the limitations of direct solver for solving large 3D problems for which the fill-in is too significant.



$n$	$N = n^3$	spaND					Direct.
		$t_F$ (s.)	$t_S$ (s.)	$n_{CG}$	$size_{Top}$	$mem_F$ ( $10^9$ )	$t_F + t_S$ (s.)
128	2 097 152	57	20	12	504	0.65	686
160	4 096 000	117	46	14	635	1.2	—
200	8 000 000	395	131	16	962	2.6	—
252	16 003 008	980	306	14	891	5.3	—

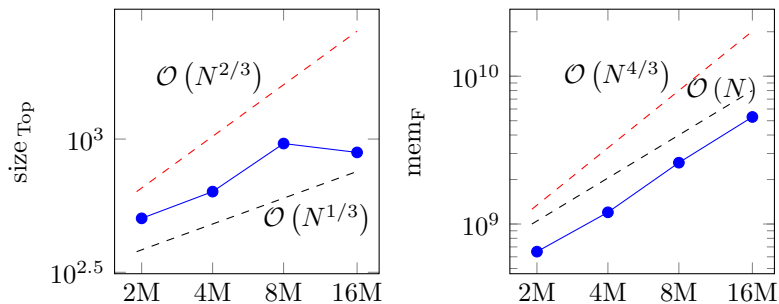


Table 4.3: SPE results. Regular geometric partitioning,  $\varepsilon = 10^{-2}$ , **OrthS**. “—” indicates the direct method ran out of memory. This problem is a regular cube, and hence very hard to solve using a direct method, since the separators are very large. spaND does not suffer from this problem and can solve this problem well, with a near (but not exactly) linear scaling with the problem size.

**4.4. Profiling.** Fig. 4.6 shows the (cumulative) memory taken by  $M$  in spaND, compared to the direct method<sup>1</sup>. This shows clearly the effect of the approximation. At the beginning, memory increases slowly. Then, we keep eliminating and going up the tree and elimination becomes more and more expensive. The sparsification, however, allows us to greatly decrease the memory use by reducing the separator’s sizes. In this specific example, sparsification is skipped for the first four levels. This can be seen on Fig. 4.6, where spaND’s level 5 memory use is slightly greater than the Direct method. After that, however, it remains almost constant.

Fig. 4.7 shows profiling (traces) when solving a larger 16M SPE problem. This clearly shows the advantage of the algorithm. When using a direct method, elimination becomes excessively slow when reaching the top of the tree, and the time spent at the last level usually dominates. For instance in this specific problem, the

<sup>1</sup>The last point of the direct method was extrapolated from a partial run

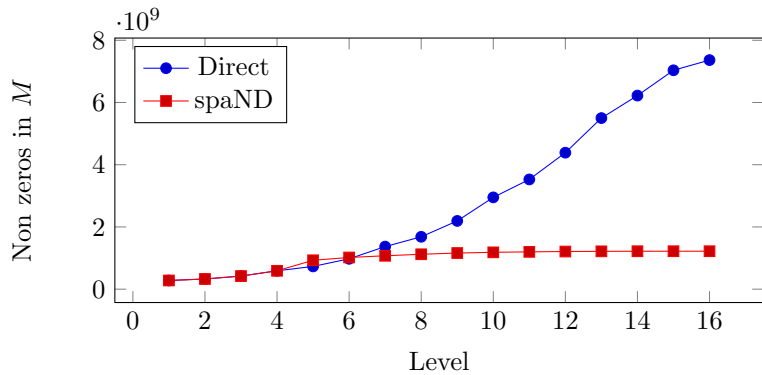


Fig. 4.6: Memory profiling of the SPE 4M problem. Each dot shows the total (cumulative) memory used by the partial preconditioner up to this level in the elimination. We compare spaND to a direct method using Nested Dissection. Thanks to the sparsification (started at level 4), the memory stays well under control, while a direct method takes more and more memory as the elimination proceeds.

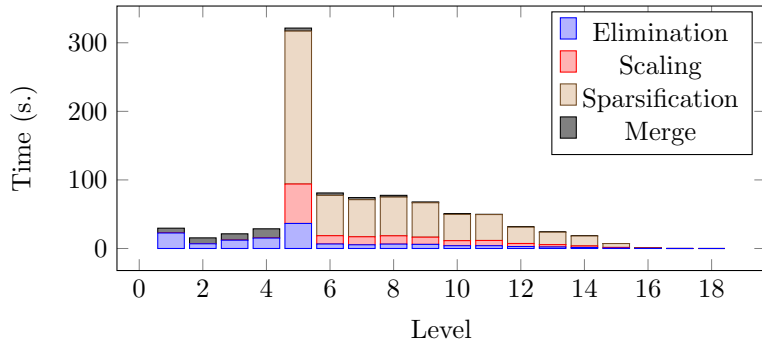


Fig. 4.7: Time profiling of the SPE 16M problem. Each bar represents the time spent at each level in the elimination. Unlike direct methods, most of the compute time is spent at the first levels (near the leaves), where we have to solve many small problems. A direct method would likely be faster at the beginning, but much slower near the end, where the fronts become very large and have to be factored exactly.

last elimination would require factoring a matrix of size approximately  $252^2 \times 252^2 = 63\,504 \times 63\,504$  (approx. 32GB!) that is completely dense. Our algorithm, on the other hand, spends more time at the early levels in the tree eliminating dofs and sparsifying separators (see the large brown bar at level 5). As a result, the time actually *decreases* as we reach higher levels in the tree. This makes for a much more efficient solver.

Notice that in this example, we start the sparsification at level 5 (i.e., we skip it for four levels). In our experiments, this gives the best results. Starting earlier leads to very high ranks (i.e., there is not much to compress), while delaying it too much leads to too large matrices  $A_{pn}$  for which RRQR becomes excessively slow.

**5. Conclusion.** In this paper we developed a sparsified Nested Dissection algorithm. The algorithm combines ideas from Nested Dissection (a fast direct method)

and low-rank approximations to reduce the separator sizes. The result is an approximate factorization that can be computed in near-linear time and results in an efficient preconditioner.

We note that it differs from the “classical” way of accelerating sparse direct solvers (like MUMPS with BLR and Pastix with HODLR). Instead of using  $\mathcal{H}$ -algebra to compress large fronts, it simply keeps the fronts small throughout the algorithm by sparsifying them at each step of the algorithm.

Prior work in this area included the HIF algorithm [36]. While our work resembles it, HIF is limited to  $n \times n \times n$  regular problems [36] and does not use either the block diagonal scaling or orthogonal transformations. The LoRaSp algorithm [42] is also similar. LoRaSp’s performances however may degrade when the ranks at the leaf level are not small and does not have the same sparsity guarantees [17]. The ordering and the ability to skip compression for some levels fixes this.

We discuss three variants of the algorithm, depending on the low-rank approximation methods (interpolative or orthogonal) and the prior use, or not, of scaling. We showed through extensive numerical experiments that the scaling has a large impact on the preconditioner’s accuracy. In addition, the use of orthogonal transformation implies that the algorithm does not break down even when  $\varepsilon \approx 1$ .

We then tested the algorithm on both ill-conditioned problems (typically hard for preconditioners) and “cubic” problems (typically hard for direct methods). On these problems, spaND is very efficient, with very favorable scaling for the factorization and near-constant CG iteration count.

Multiple research directions remain unexplored. The compression algorithm used was a simple (but still quite expensive) RRQR algorithm. Other fast algorithms could be used, like randomized methods or skeletonized interpolation (where the  $c$  of the interpolative factorization are picked a-priori using some heuristic). These techniques could greatly accelerate the compression step. The loss of accuracy remains to be studied.

Expanding the algorithm to non-SPD or non-symmetric systems is conceptually straightforward. If  $A$  is not SPD, one can simply use the  $LDL^\top$  factorization in the elimination step. Note that in this case, (symmetric) pivoting may be required and the algorithm may break down. If  $A$  is not symmetric, we need to compress  $A_{pn}$  and  $A_{np}$  and use the obtained basis on both the left and the right. The resulting preconditioner can then be coupled with GMRES instead of CG.

The partitioning algorithm is well-suited for matrices arising from the discretization of elliptic PDE’s, where we know that well-separated clusters have low-numerical rank. It would be interesting to explore other partitioning algorithms, for instance for indefinite matrices coming from Maxwell’s equations.

Finally, we mention that spaND exhibits more parallelism than direct methods. Indeed, most of the work occurs near the leaves of the tree. This means less synchronization and more parallelism. This is in contrast with direct methods based on Nested Dissection where the bottleneck is usually the factorization of the top separator at the root of the tree.

**Acknowledgement.** Some of the computing for this project was performed on the Sherlock cluster. We would like to thank Stanford University and the Stanford Research Computing Center for providing computational resources and support that contributed to these research results.

This work was partly funded by the U.S. Department of Energy National Nuclear Security Administration under Award Number DE-NA0002373-1 and partly funded

by an LDRD research grant from Sandia National Laboratories. Sandia National Laboratories is a multimission laboratory managed and operated by National Technology and Engineering Solutions of Sandia, LLC., a wholly owned subsidiary of Honeywell International, Inc., for the U.S. Department of Energy's National Nuclear Security Administration under contract DE-NA-0003525.

We thank Cindy Orozco for the idea of the modified Nested Dissection algorithm, and Bazyli Klockiewicz for his insightful comments on the numerical algorithms.

## REFERENCES

- [1] S. AMBIKASARAN, *Fast algorithms for dense numerical linear algebra and applications*, PhD thesis, Stanford University, 2013.
- [2] P. AMESTOY, C. ASHCRAFT, O. BOITEAU, A. BUTTARI, J.-Y. L'EXCELLENT, AND C. WEISBECKER, *Improving multifrontal methods by means of block low-rank representations*, SIAM Journal on Scientific Computing, 37 (2015), pp. A1451–A1474.
- [3] P. R. AMESTOY, I. S. DUFF, J.-Y. L'EXCELLENT, AND J. KOSTER, *Mumps: a general purpose distributed memory sparse solver*, in International Workshop on Applied Parallel Computing, Springer, 2000, pp. 121–130.
- [4] E. ANDERSON, Z. BAI, C. BISCHOF, L. S. BLACKFORD, J. DEMMEL, J. DONGARRA, J. DU CROZ, A. GREENBAUM, S. HAMMARLING, A. MCKENNEY, ET AL., *LAPACK Users' guide*, SIAM, 1999.
- [5] J. BARNES AND P. HUT, *A hierarchical  $\mathcal{O}(n \log n)$  force-calculation algorithm*, Nature, 324 (1986), p. 446.
- [6] M. BEBENDORF, *Efficient inversion of the galerkin matrix of general second-order elliptic operators with nonsmooth coefficients*, Mathematics of Computation, 74 (2005), pp. 1179–1199.
- [7] M. BEBENDORF AND W. HACKBUSCH, *Existence of  $\mathcal{H}$ -matrix approximants to the inverse fematrix of elliptic operators with  $l_\infty$ -coefficients*, Numerische Mathematik, 95 (2003), pp. 1–28.
- [8] M. J. BERGER AND S. H. BOKHARI, *A partitioning strategy for nonuniform problems on multiprocessors*, IEEE Transactions on Computers, (1987), pp. 570–580.
- [9] J. H. BRAMBLE, *Multigrid methods*, vol. 294, CRC Press, 1993.
- [10] A. BRANDT, S. MCCORMICK, AND J. RUGE, *Algebraic multigrid (amg) for automatic multigrid solutions with application to geodesic computations*, Report, Inst. for computational Studies, Fort Collins, Colorado, (1982).
- [11] T. F. CHAN, *Rank revealing qr factorizations*, Linear Algebra and its Applications, 88 (1987), pp. 67–82.
- [12] S. CHANDRASEKARAN, P. DEWILDE, M. GU, T. PALS, X. SUN, A.-J. VAN DER VEEN, AND D. WHITE, *Some fast algorithms for sequentially semiseparable representations*, SIAM Journal on Matrix Analysis and Applications, 27 (2005), pp. 341–364.
- [13] S. CHANDRASEKARAN, P. DEWILDE, M. GU, AND N. SOMASUNDERAM, *On the numerical rank of the off-diagonal blocks of schur complements of discretized elliptic pdes*, SIAM Journal on Matrix Analysis and Applications, 31 (2010), pp. 2261–2290.
- [14] S. CHANDRASEKARAN, M. GU, AND T. PALS, *Fast and stable algorithms for hierarchically semiseparable representations*, Submitted for publication, (2004).
- [15] S. CHANDRASEKARAN, M. GU, AND T. PALS, *A fast ULV decomposition solver for hierarchically semiseparable representations*, SIAM Journal on Matrix Analysis and Applications, 28 (2006), pp. 603–622.
- [16] Y. CHEN, T. A. DAVIS, W. W. HAGER, AND S. RAJAMANICKAM, *Algorithm 887: Cholmod, supernodal sparse cholesky factorization and update/downdate*, ACM Transactions on Mathematical Software (TOMS), 35 (2008), p. 22.
- [17] C. CHENA, L. CAMBIERA, E. G. BOMANB, S. RAJAMANICKAMB, R. S. TUMINAROB, AND E. DARVEA, *A robust hierarchical solver for ill-conditioned systems with applications to ice sheet modeling*, arXiv preprint arXiv:1811.11248, (2018).
- [18] H. CHENG, Z. GIMBUTAS, P.-G. MARTINSSON, AND V. ROKHLIN, *On the compression of low rank matrices*, SIAM Journal on Scientific Computing, 26 (2005), pp. 1389–1404.
- [19] M. CHRISTIE, M. BLUNT, ET AL., *Tenth SPE comparative solution project: A comparison of upscaling techniques*, in SPE reservoir simulation symposium, Society of Petroleum Engineers, 2001.
- [20] T. A. DAVIS AND Y. HU, *The university of florida sparse matrix collection*, ACM Transactions on Mathematical Software (TOMS), 38 (2011), p. 1.

- [21] M. FAVERGE, G. PICHON, P. RAMET, AND J. ROMAN, *On the use of H-Matrix Arithmetic in PaStiX: a Preliminary Study*, in Workshop on Fast Direct Solvers, Toulouse, France, June 2015, <https://hal.inria.fr/hal-01187882>.
- [22] R. P. FEDORENKO, *A relaxation method for solving elliptic difference equations*, Computational Mathematics and Mathematical Physics, 1 (1962), pp. 1092–1096.
- [23] W. FONG AND E. DARVE, *The black-box fast multipole method*, Journal of Computational Physics, 228 (2009), pp. 8712–8725.
- [24] A. GEORGE, *Nested dissection of a regular finite element mesh*, SIAM Journal on Numerical Analysis, 10 (1973), pp. 345–363.
- [25] P. GHYSELS, X. S. LI, F.-H. ROUET, S. WILLIAMS, AND A. NAPOV, *An efficient multicore implementation of a novel hss-structured multifrontal solver using randomized sampling*, SIAM Journal on Scientific Computing, 38 (2016), pp. S358–S384.
- [26] G. H. GOLUB AND C. F. VAN LOAN, *Matrix computations*, vol. 4, JHU Press, 2013.
- [27] L. GRASEDYCK, R. KRIEMANN, AND S. LE BORNE, *Domain decomposition based  $\mathcal{H}$ -lu preconditioning*, Numerische Mathematik, 112 (2009), pp. 565–600.
- [28] L. GREENGARD AND V. ROKHLIN, *A fast algorithm for particle simulations*, Journal of Computational Physics, 73 (1987), pp. 325–348, [https://doi.org/10.1016/0021-9991\(87\)90140-9](https://doi.org/10.1016/0021-9991(87)90140-9).
- [29] M. GU AND S. C. EISENSTAT, *Efficient algorithms for computing a strong rank-revealing qr factorization*, SIAM Journal on Scientific Computing, 17 (1996), pp. 848–869.
- [30] W. HACKBUSCH, *A sparse matrix arithmetic based on  $\mathcal{H}$ -matrices. part i: Introduction to  $\mathcal{H}$ -matrices*, Computing, 62 (1999), pp. 89–108.
- [31] W. HACKBUSCH, *Multi-grid methods and applications*, vol. 4, Springer Science & Business Media, 2013.
- [32] W. HACKBUSCH AND S. BÖRM, *Data-sparse approximation by adaptive  $\mathcal{H}^2$ -matrices*, Computing, 69 (2002), pp. 1–35.
- [33] W. HACKBUSCH AND S. BÖRM,  *$\mathcal{H}^2$ -matrix approximation of integral operators by interpolation*, Applied Numerical Mathematics, 43 (2002), pp. 129–143.
- [34] P. HÉNON, P. RAMET, AND J. ROMAN, *Pastix: a high-performance parallel direct solver for sparse symmetric positive definite systems*, Parallel Computing, 28 (2002), pp. 301–321.
- [35] M. R. HESTENES AND E. STIEFEL, *Methods of conjugate gradients for solving linear systems*, vol. 49, NBS Washington, DC, 1952.
- [36] K. L. HO AND L. YING, *Hierarchical interpolative factorization for elliptic operators: differential equations*, Communications on Pure and Applied Mathematics, 69 (2016), pp. 1415–1451.
- [37] G. KARYPIS AND V. KUMAR, *A fast and high quality multilevel scheme for partitioning irregular graphs*, SIAM Journal on scientific Computing, 20 (1998), pp. 359–392.
- [38] E. LIBERTY, F. WOOLFE, P.-G. MARTINSSON, V. ROKHLIN, AND M. TYGERT, *Randomized algorithms for the low-rank approximation of matrices*, Proceedings of the National Academy of Sciences, 104 (2007), pp. 20167–20172.
- [39] R. J. LIPTON, D. J. ROSE, AND R. E. TARJAN, *Generalized nested dissection*, SIAM Journal on Numerical Analysis, 16 (1979), pp. 346–358.
- [40] L. MIRANIAN AND M. GU, *Strong rank revealing lu factorizations*, Linear Algebra and its Applications, 367 (2003), pp. 1–16.
- [41] C. C. PAIGE AND M. A. SAUNDERS, *Solution of sparse indefinite systems of linear equations*, SIAM Journal on Numerical Analysis, 12 (1975), pp. 617–629.
- [42] H. POURANSARI, P. COULIER, AND E. DARVE, *Fast hierarchical solvers for sparse matrices using extended sparsification and low-rank approximation*, SIAM Journal on Scientific Computing, 39 (2017), pp. A797–A830.
- [43] A. PROKOPENKO, C. M. SIEFERT, J. J. HU, M. HOEMMEN, AND A. KLINVEX, *Ipack2 Users Guide 1.0*, Tech. Report SAND2016-5338, Sandia National Labs, 2016.
- [44] Y. SAAD, *Ilut: A dual threshold incomplete lu factorization*, Numerical Linear Algebra with Applications, 1 (1994), pp. 387–402.
- [45] Y. SAAD, *Iterative methods for sparse linear systems*, vol. 82, SIAM, 2003.
- [46] Y. SAAD AND M. H. SCHULTZ, *Gmres: A generalized minimal residual algorithm for solving nonsymmetric linear systems*, SIAM Journal on Scientific and Statistical Computing, 7 (1986), pp. 856–869.
- [47] Y. SAAD AND J. ZHANG, *Bilum: block versions of multielimination and multilevel ilu preconditioner for general sparse linear systems*, SIAM Journal on Scientific Computing, 20 (1999), pp. 2103–2121.
- [48] P. G. SCHMITZ AND L. YING, *A fast direct solver for elliptic problems on general meshes in 2d*, Journal of Computational Physics, 231 (2012), pp. 1314–1338.
- [49] K. STÜBEN, *A review of algebraic multigrid*, in Partial Differential Equations, Elsevier, 2001,

- pp. 281–309.
- [50] I. K. TEZAUER, M. PEREGO, A. G. SALINGER, R. S. TUMINARO, AND S. F. PRICE, *Albany/felix: a parallel, scalable and robust, finite element, first-order stokes approximation ice sheet solver built for advanced analysis*, Geoscientific Model Development (Online), 8 (2015).
  - [51] H. A. VAN DER VORST, *Bi-cgstab: A fast and smoothly converging variant of bi-cg for the solution of nonsymmetric linear systems*, SIAM Journal on scientific and Statistical Computing, 13 (1992), pp. 631–644.
  - [52] J. XIA, *Efficient structured multifrontal factorization for general large sparse matrices*, SIAM Journal on Scientific Computing, 35 (2013), pp. A832–A860.
  - [53] J. XIA, *Randomized sparse direct solvers*, SIAM Journal on Matrix Analysis and Applications, 34 (2013), pp. 197–227.
  - [54] J. XIA, S. CHANDRASEKARAN, M. GU, AND X. S. LI, *Superfast multifrontal method for large structured linear systems of equations*, SIAM Journal on Matrix Analysis and Applications, 31 (2009), pp. 1382–1411.
  - [55] J. XIA, S. CHANDRASEKARAN, M. GU, AND X. S. LI, *Fast algorithms for hierarchically semiseparable matrices*, Numerical Linear Algebra with Applications, 17 (2010), pp. 953–976.
  - [56] J. XIA AND M. GU, *Robust approximate cholesky factorization of rank-structured symmetric positive definite matrices*, SIAM Journal on Matrix Analysis and Applications, 31 (2010), pp. 2899–2920.
  - [57] J. Z. XIA, *Effective and robust preconditioning of general spd matrices via structured incomplete factorization*, SIAM Journal on Matrix Analysis and Applications, 38 (2017), pp. 1298–1322.
  - [58] K. YANG, H. POURANSARI, AND E. DARVE, *Sparse hierarchical solvers with guaranteed convergence*, arXiv preprint arXiv:1611.03189, (2016).